Molecular Dynamics of 1-Decanol in Solution Studied by NMR Coupled Relaxation and Stochastic Dynamic Simulations

Fang Liu, W. J. Horton, Charles L. Mayne, Tian-xiang Xiang, and David M. Grant*

Contribution from the Department of Chemistry, University of Utah, Salt Lake City, Utah 84112.
Received May 8, 1991

Abstract: The isotopic ^{13}C labeled 1-decanols at positions 1, 5, and 9 have been synthesized and their dynamics in $(CD_3O-CD_2CD_2)_2O$, CD_3CD_2OD, and CD_2Cl_2 solvents have been studied by ^{13}C-coupled relaxation methods. The experiments were performed in the temperature range of 245–298 K. The data were fitted using the Redfield theory of nuclear spin relaxation to yield dipolar spectral densities which were then transformed into Cartesian correlation times. The Cartesian correlation times obtained experimentally have a strong bearing on local anisotropic motion and suggest that the size of groups attached to a given carbon and also hydrogen bonding between 1-decanol and the various solvent molecules have a profound effect on local segmental motion. The hydrogen bond anchoring effect is apparently strongest near the hydrogen bonding site. The effects of solvent viscoelastic response, hydrogen bonding, and torsional forces on the motion of Cartesian modes at different locations and end-to-end vectors in 1-decanol are analyzed using both generalized (GLE) and ordinary Langevin equations (OLE) simulations. The asymmetry of Cartesian correlation times as one moves away from the chain center arises from the difference in the torsional potentials of the C–C–C–OH and C–C–C–C linkages at each end and from a hydrogen bond anchoring effect at the first carbon (C^1). The stronger retardation effect at C^1 observed in ethanol is found from the GLE simulations to be mainly attributable to a large spatial blockage of the motions of the beads near –OH. For a solute molecule surrounded by solvent molecules with internal rotation, its motion is closely correlated with the solvent relaxation rate giving significantly reduced friction forces. Conversely, the local Cartesian relaxation for 1-decanol in methylene chloride fails to correlate effectively with solvent relaxation and can be described satisfactorily by OLEs with a δ-memory kernel. The contributions from overall tumbling and internal motion to the relaxation of local Cartesian modes and to the end-to-end vectors are analyzed by using calculated apparent activation energies.

I. Introduction

Studies of chain dynamics in flexible alkyl groups, paraffin hydrocarbons, and related polymers can provide a better understanding of both segmental and overall molecular motion, especially when these substances receive both theoretical as well as experimental attention.[1] With the development of advanced computational methods, the motions of rigid molecules, small chain molecules, and even polymers now have become theoretically examinable.[2-7] Experimentally, a variety of techniques such as dielectric relaxation, ultrasonic attenuation, and infrared line shape analysis are widely used to study the dynamics of chain molecules in solution. While some of these methods provide only information about effective overall molecular motion, other techniques such as dynamic light scattering,[8-11] fluorescent dipolarization, and electron spin relaxation,[12,13] have provided additional details on local segmental motion through the direct observation of various orientational autocorrelation functions. Many optical methods require the introduction of a chromophore group covalently bonded to a specific position of the chain molecule to serve as the dynamical probe. Unfortunately, the motional perturbations created by these sizable chromophore groups on the parent molecule are usually significant and motion without the perturbation becomes difficult to assess or to calculate. In contrast, the ^{13}C coupled relaxation method is particularly versatile for the study of chain motions because of its broad range of application and because the reorientational diffusion at a specific position in the molecule is only slightly perturbed by the relatively small ^{13}C vs ^{12}C isotopic mass effect upon the chain dynamics.

Nuclear magnetic resonance (NMR) relaxation methods have proven to be powerful techniques for studying molecular dynamics and have been used widely in condensed phase and nematic systems.[14-24] Historically, single ^{13}C spin–lattice relaxation times, T_1, and transverse relaxation times, T_2, were used to describe molecular motion, but to be strictly precise such studies involving a single relaxation parameter per atom characterize only isolated nuclear spin systems. These single dynamical parameters such as T_1 or T_2 can provide at most only one effective correlation time per atom and therefore are capable of providing a single piece of "effective" molecular motional information. Only the motion of a rigid spherical molecule rotating isotropically in its environment provides the basis for such a simple model. For more complicated cases where the molecules exhibit anisotropic motion, additional diffusional parameters are required to characterize the rotations. Fortunately, the multiple ^{13}C and ^1H coupled relaxation methods exploited and applied in this study can provide valuable

(1) Bailey, R. T.; North, A. M.; Pethrick, R. A. *Molecular Motion in High Polymers*; Clarendom: Oxford, 1981.
(2) Weber, T. A. *J. Chem. Phys.* **1978**, *69*, 2347.
(3) Fixman, M. *J. Chem. Phys.* **1978**, *69*, 1527.
(4) Helfand, E. *J. Chem. Phys.* **1978**, *69*, 1010.
(5) Rebertus, D. W.; Berne, B. J.; Chandler, D. *J. Chem. Phys.* **1979**, *70*, 3395.
(6) Erman, B.; Monnerie, L. *Macromolecules* **1985**, *18*, 1985.
(7) Weber, T. A.; Helfand, E. *J. Phys. Chem.* **1983**, *87*, 2881.
(8) Perico, A.; Guenza, M. *J. Chem. Phys.* **1986**, *84*, 510.
(9) Queslel, J. P.; Erman, B.; Monnerie, L. *Macromolecules* **1985**, *18*, 1991.
(10) Viovy, J. L.; Frank, C. W.; Monnerie, L. *Macromolecules* **1985**, *18*, 2606.
(11) Viovy, J. L.; Monnerie, L.; Merola, F. *Macromolecules* **1985**, *18*, 1130.
(12) Patron, M.; Kivelson, D.; Schwartz, R. N. *J. Phys. Chem.* **1982**, *86*, 518.
(13) Noel, C.; Friedrich, C.; Monnerie, L. *Macromolecules* **1986**, *19*, 201.
(14) Mayne, C. L.; Alderman, D. W.; Grant, D. M. *J. Chem. Phys.* **1975**, *63*, 2514.
(15) Courtieu, J.; Gonord, P.; Mayne, C. L. *J. Chem. Phys.* **1980**, *72*, 953.
(16) Bernassau, J. M.; Black, E. P.; Grant, D. M. *J. Chem. Phys.* **1982**, *76*, 253.
(17) Chenon, M. T.; Bernassau, J. M.; Grant, D. M. *J. Phys. Chem.* **1982**, *86*, 2733.
(18) Fuson, M. M.; Prestegard, J. H. *J. Chem. Phys.* **1982**, *76*, 1539.
(19) Brown, M. S.; Grant, D. M.; Horton, W. J.; Mayne, C. L.; Evans, G. T. *J. Am. Chem. Soc.* **1985**, *107*, 6698.
(20) Williams, E.; Allerhand, A.; Cordes, E. H. *J. Am. Chem. Soc.* **1973**, *95*, 4871.
(21) Levy, G. C. *Acc. Chem. Res.* **1973**, *6*, 161.
(22) Vold, R. L.; Vold, R. R. *Prog. Nucl. Magn. Reson. Spectrosc.* **1972**, *12*, 79.
(23) Lyerla, J. R.; Grant, D. M. *Int. Rev. Sci.* **1972**, *4*, 155.
(24) Gara, J. F.; Desjardins, S. G.; Jones, A. A. *Macromolecules* **1981**, *14*, 64.

0002-7863/92/1514-5281$03.00/0

insights into the anisotropic motion of $^{13}CH_2$ groups in the flexible decanol chain.

1-Decanol was studied previously[25] to obtain ordinary *single* T_1 values with associated single "effective" correlation times. While this approach provides a coarse overview of chain motion, intimate details on the anisotropy are absent. The considerable conformational flexibility in 1-decanol may be expected to have a significant effect upon the motional anisotropy at various positions in the alkyl chain, and this is an important motivation for employing multiplet spin relaxation methods. In this paper, the dynamics are studied for 1-decanol ^{13}C labeled at different alkyl chain positions. The 1-decanol molecule is sufficiently large that the conformational flexibility of the chain is rich enough to allow the local segmental motion to influence strongly the relaxation, whereas in chains of less than five carbon atoms, the overall molecular motion dominates the relaxation.[26] Thus, both the overall and internal motions become important in 1-decanol. In addition, the –OH group in 1-decanol can form hydrogen bonds with oxygen-containing solvent molecules such as diglyme. The variation in the anchoring effect of hydrogen bonding at different chain positions can provide information to address the structurally dependent features on both the segmental and overall dynamics.

The study of molecular dynamics using carbon-13 coupled relaxation methods becomes either impracticable or very tedious to perform with carbon-13 at natural abundance because of its low sensitivity (^{13}C natural abundance is 1.1% compared with almost 100% ^1H) and severe overlapping of resonances in the hydrocarbon range. To overcome these drawbacks, specific carbon-13 labeling was used. Three specifically ^{13}C labeled (at the 1, 5, and 9 carbon positions) 1-decanol molecules were synthesized and thereafter studied.

An impressive progress in the theoretical development of solution dynamics[26-30] has been made in the last decade. It is becoming increasingly clear that overly simple theories are failing for molecules or molecular groups with dimensions similar to or even smaller than solvent molecules, especially when the movement is on a short time scale. For example, the OLE description, notably the Kramers theory,[31] must be generalized to incorporate short time couplings between solute molecules and their thermal bath. Although certain aspects of conformational motion in condensed phases have been dealt with by using generalized Langevin equations (GLEs),[32-35] the focus has been mainly on the role of solvent relaxation on barrier crossing rates in simple chemical reactions. It is still unclear how the solvent relaxation dynamics would affect the segmental motion in real physical systems in which a number of conformational states exist.

In our previous study of *n*-nonane and related chain molecules,[36] a numerical algorithm for solving the GLEs was developed in which the integrations over various forces were performed explicitly. These GLE simulations show that the motion of chain segments is closely correlated with solvent relaxation giving significantly reduced friction forces. The OLE model underestimates the contribution of internal motion to the relaxation of local Cartesian modes. The finite structural relaxation rate in the solvent can substantially alter not only the correlation times but the dynamic features of the relevant relaxation processes in a full GLE calculation.

In this paper, the anchoring effect of hydrogen bonding upon the motion of a chain molecule will be studied by both OLE and GLE simulations. In conjunction with the experimental results, these calculations on 1-decanol in several solvent systems determine how the motion of local segments are driven by internal torsional forces and are modified by hydrogen bonding to the solvent molecules. Furthermore, this work addresses the intriguing question of how the segment and the end-to-end dynamics of the solute molecule depend on the solvent viscoelastic properties and relaxation rates. The work also explores the extent to which the relaxation of local segments and the end-to-end vectors are affected either by the overall tumbling or by internal motions sensitive to intramolecular potentials.

The outline of this paper is as follows. The detailed experimental procedures of the isotopic syntheses and of the NMR coupled relaxation experiments are described in section II. The theoretical basis for the Brownian dynamics simulations is presented in section III. In section IV the simulations are compared with the experimental results on ^{13}C-labeled 1-decanol dissolved in various deuterated solvents. The effects of hydrogen bonding, torsional interaction, and solvent relaxation processes on the motion of various dynamic modes in 1-decanol become the principal features in the analysis.

II. Experimental Section

A. Organic Synthesis. Three 1-decanol compounds with carbon-13 incorporated into positions 1, 5, and 9, respectively, were obtained using the organic synthesis strategy shown in the schemes in the Appendix along with the detailed synthetic procedures. For the coupled relaxation study of a CH_2 spin system, 1-decanol must be enriched at only one specific position and that labeled ^{13}C atom must bear two protons. Because of the reactivity of the hydroxyl group (–OH), it must be masked during the isotopic synthesis to prevent unwanted reactions with other molecules and then restored in the final step. The low natural abundance of ^{13}C eliminates concern with background signals due to unlabeled materials with natural ^{13}C nuclear spin abundance, thereby providing completely selective observation of a specific isolated $^{13}CH_2$ moiety.

B. Sample Preparation. The samples were dissolved in $(CD_3OCD_2CD_2)_2O$, CD_3CD_2OD, and CD_2Cl_2 to yield a mole fraction concentration of about 5% in solute molecules, thereby minimizing intermolecular proton–proton interactions among solute molecules. The samples were thoroughly degassed via freeze–pump–thaw cycles and sealed in 5 mm o.d. NMR tubes.

C. NMR Experiments. The relaxation measurements were performed at 100 MHz using a Varian XL-400 spectrometer. For each spectrum, 32768 data points were acquired using a sweep width of 4618 Hz. Typically, 18 different delay times were used for each experiment, ordered randomly to reduce systematic errors. For all the experiments, the delay times used to reestablish thermal equilibrium condition were set at least 10 times the effective T_1. The experiments were performed in the temperature range of 245–298 K. The temperatures were calibrated by using methanol and the calibration accuracy was within ±0.5 K.

Four different initial perturbations of the $^{13}CH_2$ spin system are used. In the carbon-13 coupled inversion recovery experiment,[37] a carbon 180° pulse inverts all three of the carbon lines. In the proton hard pulse experiment,[37] a high-power 180° pulse at the proton resonance (applied at the middle of the proton doublet) inverts the proton doublet simultaneously. In a third class of experiments,[38] a new *J*-pulse sequence is used to create an initial condition in which the outer peaks of ^{13}C triplets are inverted 180° and the middle peak is left unperturbed. Finally, in the ^1H soft pulse experiment, a low power proton pulse[37] is used to selectively invert one of the two proton lines. Following the preparation of the nuclear spins, the system is allowed to evolve for a time τ (D_2 array), followed by a 90° observe pulse in the carbon-13 domain. The free induction decays (FID) resulting from these four experiments are collected and Fourier transformed, and the partially relaxed line intensities are measured by integrating the peak amplitudes using the Varian software. It should be indicated that the decoupler channel remains off during the FID in all experiments and is used only as a proton pulse generator during the spin preparation periods.

In the ^1H soft pulse experiment, the pulse amplitude, frequency, and duration are adjusted to produce best the 9:2:–7 magnetization distribution expected for the ideal multiplet polarization. This adjustment involves an optimization between the low power required to effect the

(25) Doddrell, D.; Allerhand, A. *J. Am. Chem. Soc.* **1971**, *93*, 1558.
(26) Grote, R. F.; Hynes, T. T. *J. Chem. Phys.* **1980**, *73*, 2715.
(27) (a) Adelman, S. A. *Adv. Chem. Phys.* **1986**, *84*, 1788. (b) Adelman, S. A. *J. Phys. Chem.* **1985**, *89*, 2213.
(28) Okuyama, S.; Oxtoby, D. W. *J. Chem. Phys.* **1986**, *84*, 5824.
(29) Zhu, S.-B.; Singh, S.; Robinson, G. W. *Phys. Rev. A* **1989**, *40*, 1109.
(30) Berne, B. J.; Tuckerman, M. E.; Straub, J. E.; Bug, A. L. R. *J. Chem. Phys.* **1990**, *93*, 5084.
(31) Kramers, H. A. *Physica (Utrecht)* **1940**, *7*, 284.
(32) Bagchi, B.; Oxtoby, D. W. *J. Chem. Phys.* **1983**, *78*, 2735.
(33) Toxvaerd, S. *J. Chem. Phys.* **1987**, *86*, 3667.
(34) Straub, J. E.; Borkovec, M.; Berne, B. J. *J. Phys. Chem.* **1987**, *91*, 4995.
(35) Zhu, S.-B.; Lee, J.; Robinson, G. W.; Lin, S. H. *J. Chem. Phys.* **1989**, *90*, 6335, 6340.
(36) Xiang, T.-X.; Liu, F.; Grant, D. M. *J. Chem. Phys.* **1991**, *95*, 7576.
(37) Mayne, C. L.; Grant, D. M.; Alderman, D. M. *J. Chem. Phys.* **1976**, *65*, 1684.
(38) Liu, F.; Mayne, C. L.; Grant, D. M. *J. Magn. Reson.* **1989**, *84*, 344.

perturbation of only one line but sufficient power to complete the spin preparation before spin relaxation processes compete with the pulse perturbations utilized in this study. The reasonably short relaxation times obtained for chain molecules require intermediate (power) soft pulses[39] in order to satisfy these conditions. The effective perturbing field is dependent on both the amplitude and offset of the radio frequency field, especially in those cases for which these two factors are comparable in magnitude. When the pulse width is set to $3^{1/2}/2J_{CH}$, the decoupling power can be adjusted so that a 360° pulse is applied to the off-resonance proton line leaving it effectively unperturbed while the on-resonance line of the doublet rotates through 180° about its effective field in the rotating frame.

The magnetizations modes are measured experimentally as a function of time and fitted with a theoretical model based on Redfield theory[40,41] to obtain the relaxation spectral densities or transition probabilities. The sum of the squares of the differences between the theoretical and experimental magnitude of M is minimized in the dynamical parameters (dipolar spectral densities and random spectral densities) using a quasi-Newton algorithm. Other parameters used to adjust for system response are also included to allow one to assess deviations from ideal spectral conditions. This symmetry adapted magnetization mode fit (MMF) method has been explicitly described previously.[37]

For the CH_2 spin system, four of the seven magnetization modes are experimentally measurable. They are (1) ${}^a\nu_C$, the total carbon magnetization, (2) ${}^a\nu_H$, the total proton magnetization, (3) ${}^a\nu_{+-+}$, the difference between the inner and the sum of the outer line intensities of the carbon triplet, and (4) ${}^s\nu_{+0-}$, the difference between the intensities of the proton doublet (also proportional to the difference in the outer two lines of the carbon triplet). The superscript labels the modes as either symmetric (s) or antisymmetric (a) under the permutation operation of spin inversion. The evolution of the magnetization modes depends on the dipolar and random spectral densities expressed explicitly in the relaxation matrices.[42] The accuracy with which the spectral densities can be measured is limited by the signal-to-noise ratio of the ^{13}C spectra from which the line intensities are determined, but the accuracy can be further enhanced by the manner in which the spin system is perturbed from equilibrium. Failure to fully prepare a given mode may leave some of the spectral densities unmeasurable or poorly determined. In previous studies, only three experiments (i.e., the proton soft pulse, the proton hard pulse, and the standard inversion–recovery experiments) were used to perturb the spin system from thermal equilibrium.[37] As a consequence of these experiments, a maximum perturbation is created for the ${}^s\nu_{+0-}$, ${}^a\nu_H$, and ${}^a\nu_C$ modes, respectively, depending upon the experiment. However, considerable difficulty has been encountered in perturbing the ${}^a\nu_{+-+}$ mode from its thermal equilibrium states in previous studies. The *new J*-pulse sequence, developed in this study, perturbs this specific mode in an optimal way. Significant improvement in the accuracy of the fits is achieved by adding these data from the J-pulse experiments,[38] and the marginal standard deviations for $J_{HH'}$ and j_H are reduced substantially. Furthermore, unfavorable correlations between pairs ($J_{HH'HH'}$, $j_{HH'}$) and (j_H, $j_{HH'}$) of spectral densities are also reduced remarkably by inclusion of the new experimental data. Inclusion of J-pulse data also makes the computer fitting procedure converge more rapidly. The greater perturbation created for the ${}^a\nu_{+-+}$ mode with the J-pulse, particularly at short times, opens relaxation channels in the coupled differential equations with a stronger dependence on $J_{HH'HH'}$, j_H, and $j_{HH'}$, and these constraints decrease correlations between $J_{HH'HH'}$ and $j_{HH'}$ and between j_H and $j_{HH'}$ which otherwise impair their independent determination from the experimental data.[38]

The least-square fits of the different experimental results are shown in Figure 1 for 1-decanol-*1*-^{13}C dissolved in deuterated diglyme at 273 K. Parts A–E of Figure 1 correspond to the results of the soft pulse, hard pulse, inversion recovery, and $+J$-pulse and $-J$-pulse experiments, respectively. The scale of the total carbon magnetization is normalized to unity under the thermal equilibrium condition. In the figures the points are the experimental data while the lines are the results of the least-squares fitting of the coupled differential equations. Only the experimentally measurable modes for each experiment have been plotted. The difference between the experimental points and calculated fit is less than 1% of the total carbon magnetization. As Figure 1 shows, the experiments have been designed to give a maximum perturbation for each of the modes measured.

In Figure 1B, the ${}^s\nu_{+0-}$ mode deviates from zero by about 4% when the delay time, D_2, equals T_1 and then relaxes back to zero. This phenomenon indicates a relatively small coupling effect between chemical shift anisotropy (csa) and dipolar interaction in this particular system. Further study on the dipolar/csa effect is under progress for other alcohols where this interference term appears to be significantly larger.[43]

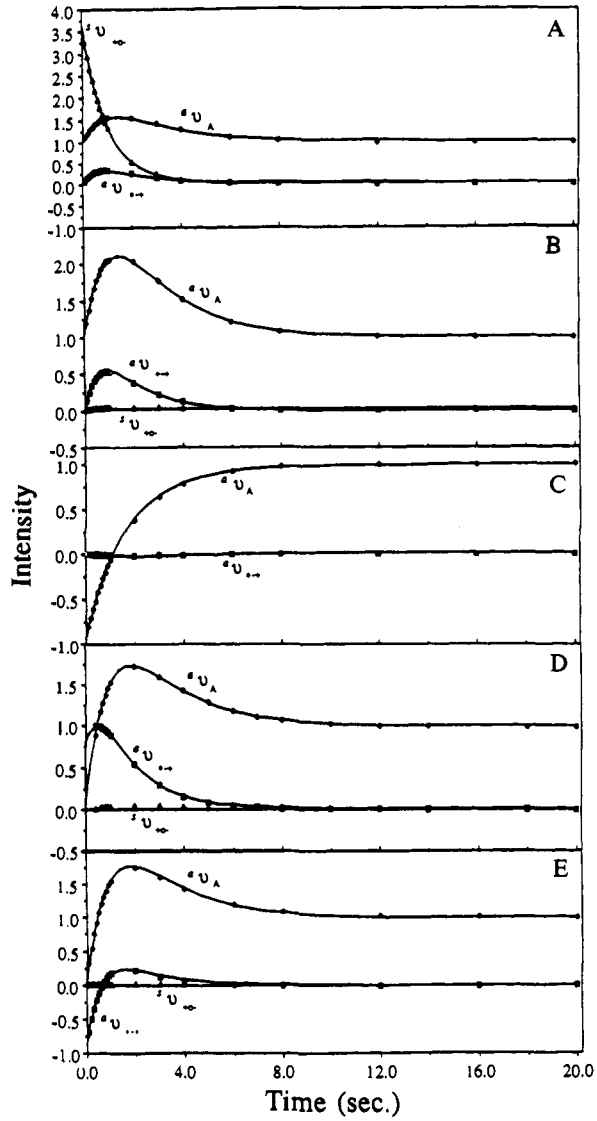

Figure 1. Partial results of nonlinear least-squares fits of the data on $CH_3(CH_2)_8{}^{13}CH_2OH$ in deuterated diglyme at 273 K: A, for the proton soft pulse experiment; B, for the proton hard pulse experiment; C, for the coupled inversion recovery experiment; D, for the $+J$-pulse experiment; E, for the $-J$-pulse experiment.

Since the overall rotation and the internal motion for molecules like 1-decanol in solutions have relaxation rates much greater than the reciprocal of the Larmor frequency of the NMR spectrometer, the resonances of such systems are observed in the extreme narrowing limit, $(\omega\tau)^2 \ll 1$. In this limiting regime, the dipolar relaxations of a methylene group $^{13}CH_2$ can be described in terms of four dipolar spectral densities (J_{CHCH}, $J_{HH'HH'}$, $J_{CHCH'}$, and $J_{CHHH'}$). The other interactions are all included into random field terms (i.e., carbon autocorrelation random spectral densities, j_C, and the proton auto- and cross-correlation random field densities j_H and $j_{HH'}$, respectively).

The dynamic behavior of 1-decanol has been studied in the following three solvent systems: (1) perdeuterated diglyme, a hydrogen bond acceptor capable of forming one hydrogen bond with one 1-decanol (in addition, it has nine chain segments which is comparable in length with 1-decanol); (2) perdeuterated ethanol, an highly associated solvent capable of forming more than one hydrogen bond between the 1-decanol and the solvent; (3) perdeuterated methylene chloride, a negligible hydrogen bonding solvent.

The values of the spectral densities obtained for each ^{13}C labeled sample dissolved in these three solvents at several temperatures are listed in Tables I–III along with their estimated marginal standard deviations

(39) Bovee, W. M. M. *Mol. Phys.* **1975**, *29*, 1673.
(40) Redfield, A. G. *IBM J. Res. Dev.* **1957**, *1*, 19.
(41) Redfield, A. G. *Adv. Magn. Reson.* **1965**, *1*, 1.
(42) Werbelow, L. G.; Grant, D. M. *Adv. Magn. Reson.* **1977**, *9*, 189.
(43) Unpublished result.

Table I. Values of the Fitted Parameters Obtained from Fits of the Relaxation Data of ^{13}C-Labeled (1, 5, and 9 Positions) 1-Decanol in Deuterated Diglyme

temp, K	J_{CHCH}	$J_{HH'HH'}$	$J_{CHCH'}$	$J_{CHHH'}$	j_H	carbon position
241	0.216 ± 0.002	0.180 ± 0.006	0.003 ± 0.006	0.123 ± 0.003	0.10 ± 0.01	1
	0.271 ± 0.002	0.22 ± 0.01	0.059 ± 0.006	0.179 ± 0.003	0.22 ± 0.02	5
	0.148 ± 0.001	0.146 ± 0.006	0.018 ± 0.004	0.094 ± 0.002	0.08 ± 0.01	9
250	0.186 ± 0.002	0.160 ± 0.006	0.006 ± 0.005	0.104 ± 0.002	0.08 ± 0.01	1
	0.217 ± 0.002	0.159 ± 0.008	0.054 ± 0.005	0.139 ± 0.002	0.16 ± 0.02	5
	0.114 ± 0.001	0.118 ± 0.005	0.017 ± 0.004	0.069 ± 0.001	0.05 ± 0.01	9
261	0.121 ± 0.001	0.110 ± 0.005	0.000 ± 0.004	0.072 ± 0.001	0.08 ± 0.01	1
	0.159 ± 0.001	0.114 ± 0.007	0.035 ± 0.004	0.104 ± 0.002	0.13 ± 0.01	5
263	0.082 ± 0.001	0.086 ± 0.003	0.008 ± 0.003	0.050 ± 0.001	0.038 ± 0.006	9
273	0.093 ± 0.001	0.082 ± 0.003	−0.001 ± 0.002	0.053 ± 0.001	0.048 ± 0.005	1
	0.117 ± 0.001	0.100 ± 0.004	0.027 ± 0.003	0.079 ± 0.001	0.09 ± 0.01	5
	0.059 ± 0.001	0.066 ± 0.004	0.004 ± 0.003	0.036 ± 0.001	0.027 ± 0.006	9
298	0.049 ± 0.001	0.043 ± 0.002	0.002 ± 0.001	0.028 ± 0.001	0.028 ± 0.003	1
	0.065 ± 0.001	0.050 ± 0.005	0.009 ± 0.003	0.043 ± 0.001	0.05 ± 0.01	5
	0.035 ± 0.001	0.037 ± 0.001	0.001 ± 0.001	0.021 ± 0.001	0.016 ± 0.002	9

Table II. Values of the Fitted Parameters Obtained from Fits of the Relaxation Data of ^{13}C-Labeled (1, 5, and 9 Positions) 1-Decanol in Deuterated Ethanol

temp, K	J_{CHCH}	$J_{HH'HH'}$	$J_{CHCH'}$	$J_{CHHH'}$	j_H	carbon position
247.6	0.247 ± 0.003	0.196 ± 0.009	0.047 ± 0.008	0.168 ± 0.004	0.08 ± 0.02	1
	0.193 ± 0.002	0.154 ± 0.009	0.046 ± 0.005	0.133 ± 0.002	0.16 ± 0.02	5
	0.096 ± 0.001	0.093 ± 0.003	0.013 ± 0.002	0.061 ± 0.001	0.048 ± 0.005	9
257.6	0.192 ± 0.002	0.161 ± 0.007	0.040 ± 0.007	0.129 ± 0.002	0.05 ± 0.01	1
	0.154 ± 0.001	0.123 ± 0.005	0.037 ± 0.003	0.103 ± 0.002	0.12 ± 0.01	5
	0.073 ± 0.001	0.070 ± 0.002	0.009 ± 0.002	0.047 ± 0.001	0.038 ± 0.004	9
270.3	0.148 ± 0.001	0.125 ± 0.005	0.029 ± 0.006	0.098 ± 0.002	0.04 ± 0.01	1
	0.121 ± 0.001	0.093 ± 0.004	0.027 ± 0.003	0.081 ± 0.001	0.10 ± 0.01	5
	0.055 ± 0.001	0.058 ± 0.002	0.004 ± 0.002	0.035 ± 0.001	0.026 ± 0.003	9
298	0.084 ± 0.001	0.069 ± 0.002	0.016 ± 0.003	0.056 ± 0.001	0.028 ± 0.004	1
	0.071 ± 0.001	0.058 ± 0.003	0.015 ± 0.002	0.048 ± 0.001	0.059 ± 0.007	5
	0.032 ± 0.001	0.025 ± 0.001	0.004 ± 0.001	0.020 ± 0.001	0.026 ± 0.002	9

Table III. Values of the Fitted Parameters Obtained from Fits of the Relaxation Data of ^{13}C-Labeled (1, 5, and 9 Positions) 1-Decanol in Deuterated Methylene Chloride

temp, K	J_{CHCH}	$J_{HH'HH'}$	$J_{CHCH'}$	$J_{CHHH'}$	j_H	carbon position
245.5	0.107 ± 0.001	0.125 ± 0.005	0.012 ± 0.004	0.065 ± 0.001	0.060 ± 0.006	1
	0.097 ± 0.001	0.095 ± 0.004	0.014 ± 0.002	0.055 ± 0.001	0.070 ± 0.007	5
	0.059 ± 0.001	0.054 ± 0.002	0.001 ± 0.002	0.035 ± 0.001	0.034 ± 0.004	9
258.0	0.078 ± 0.001	0.082 ± 0.004	−0.002 ± 0.002	0.046 ± 0.001	0.063 ± 0.005	1
	0.074 ± 0.001	0.065 ± 0.004	0.007 ± 0.002	0.043 ± 0.001	0.057 ± 0.006	5
	0.045 ± 0.001	0.042 ± 0.002	0.000 ± 0.001	0.027 ± 0.001	0.026 ± 0.003	9
269.7	0.054 ± 0.001	0.056 ± 0.002	−0.004 ± 0.001	0.031 ± 0.001	0.051 ± 0.005	1
	0.058 ± 0.001	0.046 ± 0.003	0.007 ± 0.002	0.033 ± 0.001	0.050 ± 0.004	5
	0.036 ± 0.001	0.033 ± 0.001	0.000 ± 0.001	0.021 ± 0.001	0.020 ± 0.002	9
282.5	0.039 ± 0.001	0.043 ± 0.002	0.000 ± 0.001	0.019 ± 0.001	0.036 ± 0.002	1
	0.047 ± 0.001	0.036 ± 0.003	0.006 ± 0.001	0.027 ± 0.001	0.041 ± 0.006	5
	0.029 ± 0.001	0.029 ± 0.001	0.000 ± 0.001	0.017 ± 0.001	0.015 ± 0.002	9
297.8	0.030 ± 0.001	0.031 ± 0.002	−0.002 ± 0.001	0.015 ± 0.001	0.028 ± 0.003	1
	0.038 ± 0.001	0.030 ± 0.003	0.004 ± 0.001	0.022 ± 0.001	0.032 ± 0.005	5
	0.023 ± 0.001	0.021 ± 0.001	0.000 ± 0.001	0.013 ± 0.001	0.014 ± 0.001	9

in the fit. As expected, the dipolar spectral densities decrease as the temperature increases. For the temperature ranges used in this CH_2 coupled relaxation study, the dipole–dipole interaction is either a dominant or at least a principal mechanism for spin relaxation. As the temperature increases, the rates of various molecular motions increase, which quenches the efficiency of the dipolar interactions and reduces the magnitude of the dipolar spectral densities at higher temperatures. The errors intrinsic in the measurement appear to remain at the same level independent of temperature, making this method considerably more accurate at lower temperatures where the dipolar densities are larger. Unfortunately, the solubility of the compound places a lower limit on the experimental temperatures that can be achieved. In the spectral analysis, j_C is locked to zero since its value was always within one marginal standard deviation of zero when this parameter was allowed to vary.

The spectral densities of greatest relevance, J_{CHCH}, $J_{CHCH'}$, $J_{CHHH'}$, and $J_{HH'HH'}$, which are the zero-frequency Laplace transforms of the corresponding time correlation functions, describe the reorientation rates of internuclear dipole vectors at a given time relative to its position at a specified earlier time. The autocorrelation spectral densities (J_{CHCH}, $J_{HH'HH'}$) correspond to the diagonal elements in the relaxation matrix and are directly related to the effective spin–lattice relaxation time measured for proton decoupled spectra. However, it is difficult to give a simple interpretation for the cross-correlated dipolar terms ($J_{CHCH'}$, $J_{CHHH'}$). It is convenient to transform[44] the dipolar spectral densities into model-independent quantities, the Cartesian correlation times (τ_{xx}, τ_{yy}, τ_{zz}, and τ_{xy}), commonly used in statistical mechanics of flexible chains as follows

$$\tau_{xx} = \frac{3}{2\alpha^4}\left\{\frac{1}{2}(J'_{CHCH} + J'_{CHCH'}) + \beta^4 J'_{HH'HH'} - 2\beta^2 J'_{CHHH'}\right\} \quad \text{(II.1a)}$$

$$\tau_{yy} = \frac{3}{2} J'_{HH'HH'} \quad \text{(II.1b)}$$

$$\tau_{zz} = \frac{3}{2\alpha^4}\left\{\frac{1}{2}(J'_{CHCH} + J'_{CHCH'}) + (\alpha^2 - \beta^2)^2 J'_{HH'HH'} + 2(\alpha^2 - \beta^2) J'_{CHHH'}\right\} \quad \text{(II.1c)}$$

$$\tau_{xy} = \frac{1}{4\alpha^2\beta^2}(J'_{CHCH} - J'_{CHHH'}) \quad \text{(II.1d)}$$

(44) Fuson, M. M.; Brown, M. S.; Grant, D. M.; Evans, G. T. *J. Am. Chem. Soc.* **1985**, *107*, 6695.

where $\alpha = \cos(\theta/2)$, $\beta = \sin(\theta/2)$, and θ is the HCH′ angle. The J' reduced power densities are obtained from the respective dipolar J's as

$$J'_{ijkl} = \frac{20}{9K_{ijkl}} J_{ijkl}(\omega = 0) \qquad \text{(II.2)}$$

where $K_{ijkl} = \gamma_i\gamma_j\gamma_k\gamma_l\hbar^2/r_{ij}^3 r_{kl}^3$. The multiplicatioin by $20/9K$ in eq II.2 converts the J power densities from frequency units into the corresponding dipolar times, J'_{ijkl}, given in eq II.2. In this more common Cartesian representation, assumptions about the structure and dynamics of the molecular system are avoided. The geometrical parameters needed in the transformation to the Cartesian frame for typical alkyl chains are CH bond length of 1.12 Å and the HCH′ bond angle of 108.5°. These structure parameters were obtained from electron diffraction data on a small alkane.[45]

III. Brownian Dynamics Simulations

A. Generalized Langevin Equations. In a dilute solution (i.e., the condition which obtains in the experimental measurements), the stochastic equations of motion for a *single* solute molecule with $N + 1$ interacting beads (i.e., GLEs) can be written as[46]

$$m_i \frac{d\mathbf{v}_i(t)}{dt} = \mathbf{P}_i(t) - \int_0^t dt' \, \xi_i(t') m_i \mathbf{v}_i(t - t') + \mathbf{R}_i(t) \qquad \text{(III.1)}$$

$$i = 1, 2, ..., N + 1$$

where $\mathbf{v}_i$ is the Cartesian velocity of bead i in a laboratory-fixed frame. $\mathbf{P}_i(t)$ is the internal potential force between bead i and all the other beads in the chain and may incorporate potentials of mean force due to the static interaction with the solvent.[46] The convolution integral of the velocity $\mathbf{v}_i(t)$ with a time-dependent memory function $\xi_i(t)$ is the friction force $\mathbf{F}_i(t)$. $\mathbf{R}_i(t)$ is a random force with vanishing mean. Neglecting cross correlation between the random force $\mathbf{R}_i(t)$ and the potential force $\mathbf{P}_i(t)$, the following dissipation–fluctuation relation[46] is obtained

$$6m_i kT\xi_i(t) = \langle \mathbf{R}_i(0)|\mathbf{R}_i(t)\rangle \qquad \text{(III.2)}$$

In the OLE description, a Dirac-δ function is used for the memory kernel $\xi_i(t)$, i.e., $\xi_i(t) = \xi_{i,o}\delta(t)$.

In order to solve the GLEs, an appropriate hydrodynamic theory must be used. For hydrocarbon chain molecules in organic solutions, van der Waals forces are the dominant interaction mechanisms and the slip boundary condition is a good approximation. Following our previous study,[36] the frictional function $\xi(s)$ for translational motion of a sphere with radius r is given in the Laplace plane ($s = i\omega$) by the relationship

$$\xi(s) = 4\pi\eta_s(s) r_e \qquad \text{(III.3)}$$

where r_e is an effective hydrodynamic radius given by

$$r_e = \frac{r}{1 + (\eta_s/3\eta_l)} \qquad \text{(III.4)}$$

The longitudinal viscosity η_l is related to the shear velocity of η_s and bulk viscosity η_v by, $\eta_l = (^4/_3)\eta_s + \eta_v$. For rotational motion of a sphere, no friction is experienced when the perfect "slip" condition is assumed.

The solvent viscoelastic response is dependent on various relaxation mechanisms of solvent molecules.[47] One simple model[48] considers mode relaxations as independent processes and the solvent response can then be decomposed into separate terms

$$\eta_s(s) = G_\infty \sum_i \frac{C_{is}}{(\omega_{is} + s)} \qquad \text{(III.5)}$$

where G_∞ is the infinite frequency shear modulus, C_{is} is the normalized relaxation amplitude, and ω_{is} is the relaxation frequency associated with mode i.

To determine the dynamical parameters involved in eq III.5, Sceat's evaluation[48] of viscoelastic properties of n-alkane liquids is used in the following ansatz for solvents with internal rotation: (1) $C_{ss} \approx 1.0$; (2) $C_{vs}/\omega_{vs} = 0.0$; (3) $(C_{is}/\omega_{is}) + (C_{rs}/\omega_{rs}) = 0.5(C_{ss}/\omega_{ss})$; (4) $C_{is} + C_{rs} \ll 1$. These relations indicate that the structural relaxation mode is the dominant channel in determining the frequency-dependent shear viscosity.

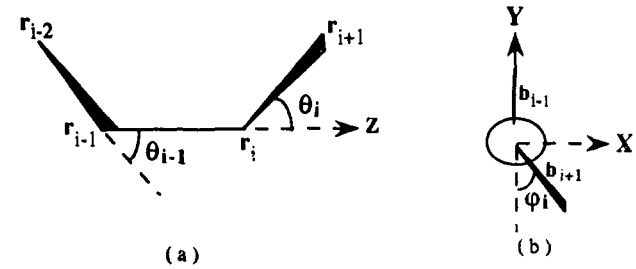

Figure 2. Schematic drawings of a portion of a chain molecule illustrating the definitions of the coordinate variables.

Table IV. Geometrical and Interaction Parameters Used in the Computer Simulations

b_0, Å		θ_0, deg	
C–O	1.43	CCO	108
C–C	1.54	CCC	112
k_b, J/(mol Å^2)		k_θ, J/mol	
C–C	9.3×10^5	CCO	1.3×10^5
C–O	9.3×10^5	CCC	1.3×10^5
σ, Å		ϵ, kcal/mol	
O···O	3.07	0.17	
CH_n···CH_n	3.92	0.14	

The random force on bead i, $\mathbf{R}_i(t)$, is composed of n parts

$$\mathbf{R}_i(t) = \sum_{j=1}^{n} R_{ij}(t) \qquad \text{(III.6)}$$

where $\mathbf{R}_{ij}(t)$ is the random force exerted by a distinct solvent relaxation mode j. As different relaxation modes are assumed to be independent, then

$$\langle \mathbf{R}_{ij}(0)|\mathbf{R}_{ij'}(t)\rangle = 0 \qquad \text{(III.7)}$$

$$j \neq j'$$

Substituting eqs III.6 and III.7 into eq III.2, one has

$$6m_i kT\xi_{ij}(t) = \langle \mathbf{R}_{ij}(0)|\mathbf{R}_{ij}(t)\rangle \qquad \text{(III.8)}$$

where

$$\xi_{ij}(t) = \omega_{js}\xi_{0,ij}e^{-\omega_{js}t} \qquad \text{(III.9)}$$

$$t \geq 0$$

and the frictional coefficient $\xi_{o,ij}$ is equal to $4\pi r_e G_\infty C_{js}/\omega_{js}$.

B. Molecular Model. In this study, a 1-decanol molecule is represented as a collection of interacting beads with methylene, methyl, and hydroxyl groups being modeled as extended atoms. A flexible chain model is employed, since previous studies[49,50] have shown that the use of holonomic constraints on the bond stretch and bend vibration may substantially alter the statistical weight of different rotamer states and severely modify the course of isomerization processes. The definitions of the relevant dynamic variables are shown in Figure 2. The bond length b_i between beads i and $i - 1$ and the angle θ_i at vertex i between the bond $\mathbf{b}_{i-1}$ and $\mathbf{b}_i$ are kept, respectively, near the equilibrium bond length b_0 and angle θ_0 with the following harmonic potentials

$$V_{C\text{-}C}(b_i) = \frac{1}{2}k_b(b_i - b_0)^2 \qquad \text{(III.10)}$$

$$V_{CCC}(\theta_i) = \frac{1}{2}k_\theta(\cos\theta_i - \cos\theta_0)^2 \qquad \text{(III.11)}$$

where k_b and k_θ are the force constants for bond stretch vibration and for bond bending vibration, respectively. The structural and

(45) Bonham, R. A.; Bartell, L. S.; Kohl, D. A. *J. Am. Chem. Soc.* **1959**, *81*, 4765.
(46) Xiang, T.-X.; Liu, F.; Grant, D. M. *J. Chem. Phys.* **1991**, *94*, 4463.
(47) MacPhail, R. A.; Kivelson, D. *J. Chem. Phys.* **1984**, *80*, 2102.
(48) Sceats, M. G.; Dawes, J. M. *J. Chem. Phys.* **1985**, *83*, 1298.
(49) Fixman, M. *Proc. Natl. Acad. Sci. U.S.A.* **1974**, *71*, 3050.
(50) Helfand, E. *J. Chem. Phys.* **1979**, *71*, 5000.

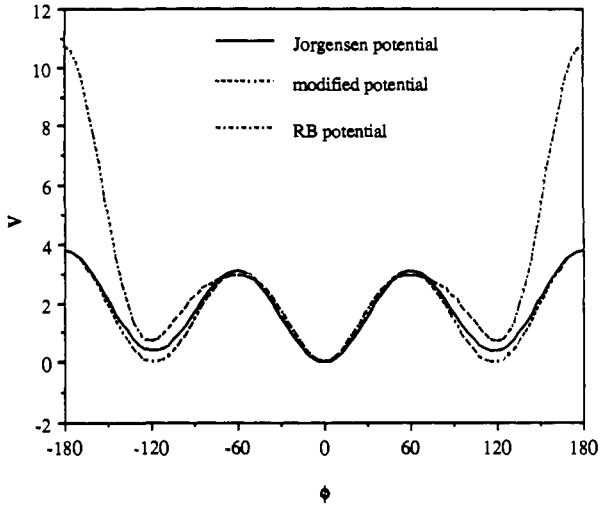

Figure 3. The R–B torsional potential, the Jorgensen 1-propanol potential, and our modified Jorgensen potential as a function of dihedral angle.

interaction parameters used in the simulations are summarized in Table IV.

The local isomerization movement is driven to a large extent by torsional forces. Hence, a critical step is to choose appropriate torsional potentials for dihedral angles $\{\phi_i, i = 1, 2, ..., N-2\}$. For the C–C–C–C linkages, their evolution is governed by the Ryckaert–Bellemans (R–B) potential[51]

$$V(\phi)/k_B = 1.116 + 1.462\cos\phi - 1.578\cos^2\phi - 0.368\cos^3\phi + 3.156\cos^4\phi - 3.788\cos^5\phi \text{ (kcal/mol)} \quad \text{(III.12)}$$

in which the trans–gauche barrier is 2.95 kcal/mol, the trans–gauche energy gap is 0.70 kcal/mol, and the restrictive trans–cis energy difference is 10.7 kcal/mol.

Jorgensen's 1-propanol torsional potential is[52]

$$V(\phi) = 1.669 + 4.239\cos\phi + 0.212\cos^2\phi - 6.12\cos^3\phi \text{ (kcal/mol)} \quad \text{(III.13)}$$

with a trans–gauche barrier of 3.07 kcal/mol, a trans–gauche energy defect of 0.37 kcal/mol, and a trans–cis energy difference of 3.76 kcal/mol. The Jorgensen potential has a nearly symmetric 3-fold barrier and thus the passage over the cis barrier is more likely than for the R–B potential. In the presence of hydrogen bonding at C^1, the torsional transitions among trans, gauche$_+$, and gauche$_-$ states could become more difficult due to the spatial hindrance of hydrogen-bonded solvent molecules and solvent packing.

A modified Jorgensen torsional potential for the C–C–C–OH linkage in 1-decanol was observed to give better simulation results in comparison with our NMR experimental data (see section IV)

$$V'(\phi) = 1.42 + 4.72\cos\phi + 0.46\cos^2\phi - 6.6\cos^3\phi \text{ (kcal/mol)} \quad \text{(III.14)}$$

In eq III.14 the trans–gauche and trans–cis energy barriers remain the same as in the Jorgensen torsional potential, while the trans–gauche energy difference is changed from 0.37 to 0.0 kcal/mol, making the energy of the gauche states equal to that of the trans state. This change in equilibrium population decreases τ_{zz} since the projection of the z direction in gauche states fails to lie along the backbone of the chain. Increased correlation times are noted for the other Cartesian modes whose orientations now project more along the long axis of the chain in gauche states. Figure 3 plots the R–B potential, Jorgensen 1-propanol potential, and our modified potential as a function of dihedral angle.

The effect of exclusive volume (i.e., two or more beads remote from one another along the chain cannot occupy the same volume element at the same time) is taken into account by imposing Lennard-Jones (6–12) potentials between extended atoms separated further than the third nearest neighbors

$$V_{ij} = 4\epsilon_{ij}\left\{\left(\frac{\sigma_{ij}}{r_{ij}}\right)^{12} - \left(\frac{\sigma_{ij}}{r_{ij}}\right)^{6}\right\} \quad \text{(III.15)}$$

The length and energy parameters of the Lennard-Jones (L-J) potentials are listed in Table IV. For interactions between different beads the following combining rules are used

$$\sigma_{ij} = \frac{1}{2}(\sigma_{ii} + \sigma_{jj}) \text{ and } \epsilon_{ij} = (\epsilon_{ii}\epsilon_{jj})^{1/2}$$

The sphere radii (r) for the extended atoms can be deduced from the slip boundary conditions. In the limit of perfect "slip", the normal component of the fluid velocity is equal to the normal component of velocity of the sphere on the spherical surface, while the fluids have no tangential component of the normal stress on the surface. These conditions can be satisfied when the intermolecular force normal to the surface is zero. If the sphere interacts via Lennard-Jones (6–12) potentials (V_{ij}), then $r = 2^{1/6}\sigma$, and sphere radii of 2.20 and 1.95 Å are obtained for $-CH_n$ and –OH, respectively. As the sphere radii are greater than the relevant bond lengths (cf. Table IV), a considerable portion of the surface area of each bead is buried by its neighbors. These van der Waals spheres are then represented by a set of equivalent nonoverlapping spheres with smaller radii whose surface areas equal the exposed surface areas of the original van der Waals spheres.[53] By analyzing the geometrical structure of 1-decanol chain, we find that independent of the conformational states of the chain molecule, the effective radii of r(OH) = 1.45 Å, $r(H_2C\text{-}1)$ = 1.43 Å, $r(H_2C\text{-}2)$ = 1.27 Å, $r(H_2C\text{-}n)$ = 1.25 Å (for n = 3–8), $r(H_2C\text{-}9)$ = 1.32 Å, and $r(H_3C\text{-}10)$ = 1.76 Å, where the n in (C-n) denotes the carbon position in the chain.

C. Hydrogen Bonding Dynamics. A two-state hydrogen bonding dynamics model (one state is a hydrogen-bond-free state and the other a hydrogen-bonded state) is adopted in the simulations

$$\text{ROH} + \text{M} \underset{k_b}{\overset{k_f}{\rightleftharpoons}} \text{ROH}\cdots\text{M} \quad \text{(III.16)}$$

In proposing this two-state hydrogen bond model, it is assumed that the short-time details on the time scale of a vibrational period lack importance in the relatively long-time dynamics of molecular conformational motion. This assumption should be valid in the present case because the small-amplitude vibration of hydrogen bonds have a negligible effect on the frictional drag of the –OH segment. The hydrogen bonding state is characterized with a stochastic variable, $\chi(t)$, which can take the values 0 and 1 in the two-state model. Its value is uniquely determined by the following conditional probabilities $P(\chi=i,t|\chi=i,0)$ (i = 0 or 1), with two parameters, k_f and k_b, the rate constants for hydrogen bond formation and breaking, respectively

$$P(\chi=0,t|\chi=0,0) = e^{-k_f t} \quad \text{(III.17a)}$$

$$P(\chi=1,t|\chi=1,0) = e^{-k_b t} \quad \text{(III.17b)}$$

The ratio of k_f to k_b is given by the equilibrium relation

$$\frac{1-p_B}{p_B} = \frac{k_f}{k_b} \quad \text{(III.18)}$$

where p_B is the probability that a randomly selected hydrogen bond is intact. It is seen that the decay of the state with i (i = 0 or 1) intact hydrogen bonds follows a Poisson distribution. The times for changing the hydrogen bonding state are obtained in the computer simulations from a random number generator to be consistent with the corresponding independent Poisson distributions.

(51) Ryckaert, J. P.; Bellemans, A. *Chem. Phys. Lett.* **1975**, *30*, 123.
(52) Jorgensen, W. L. *J. Phys. Chem.* **1986**, *90*, 1276.
(53) Pastor, R. W.; Karplus, M. *J. Phys. Chem.* **1988**, *92*, 2636.

The stationary probability of i intact hydrogen bonds, $P_{s,i}$, is given by

$$P_{s,1} = p_B \tag{III.19a}$$

$$P_{s,0} = 1 - p_B \tag{III.19b}$$

from which the initial state of hydrogen bonding at the start of a trajectory run is sampled.

If the solvent molecule is not a hydrogen-bond donor (e.g., diglyme), only one hydrogen bond per solute molecule is possible and the two-state model can accurately describe the hydrogen bonding dynamics between the labeled solute molecule and the surrounding solvent molecules. For hydrogen bonding between a 1-decanol molecule and associated solvent molecules (e.g., ethanol), both species can act as hydrogen-bond acceptors as well as hydrogen-bond donors. As a result, more than one hydrogen bond per solute molecule is possible. In such a circumstance, the two-state model only provides an approximate description of the true dynamic processes and requires the use of an effective friction constant for the hydrogen bonded –OH bead.

The hydrogen bonding dynamics are treated by enlarging the related GLEs (cf. eq III.1) to include the overall translational motion of a virtual body v whose dynamic parameters are a function of $\chi(t)$

$$m_1 \frac{d^2\mathbf{r}_1(t)}{dt^2} = \mathbf{P}^1(t) - \frac{\partial V_{HB}}{\partial r_1} - \int_0^t dt' \, \xi_1(t')\mathbf{v}_1(t-t') + \mathbf{R}_1(t) \tag{III.20a}$$

$$m_i \frac{d^2\mathbf{r}_i(t)}{dt^2} = \mathbf{P}_i(t) - \int_0^t dt' \, \xi_i(t')\mathbf{v}_i(t-t') + \mathbf{R}_i(t) \tag{III.20b}$$

$$i = 2, 3, ..., N+1$$

$$m_v \frac{d^2\mathbf{r}_v(t)}{dt^2} = -\frac{\partial V_{HB}}{\partial r_v} - \int_0^t dt' \, \xi_v(t')\mathbf{v}_v(t-t') + \mathbf{R}_v(t) \tag{III.20c}$$

where $\{\mathbf{r}_1, \mathbf{v}_1\}$ denotes the coordinates for the –OH bead in 1-decanol and $\{\mathbf{r}_v, \mathbf{v}_v\}$ represents the corresponding coordinates for the virtual body which interacts via a hydrogen bond potential $\mathbf{V}_{HB}$ with the –OH group. $\mathbf{R}_v(t)$ is the stochastic force exerted by the solvent on the virtual body v. The coupling of translational and rotational motions of hydrogen bonded solvent molecules is excluded, as the rotation of the virtual body would distort the optimum configuration (usually near linear) of the hydrogen bond and thus would require substantial amounts of energy. The structural effect of hydrogen-bonded solvent molecules due to their conformational motion is not considered explicitly but is averaged in the effective friction force imposed on the virtual body. The microscopic features in eqs III.20 are described by the stochastic variable $\chi(t)$.

Instead of using complete differential equations in the simulations, contracted equations of motion are used by invoking the adiabatic elimination of fast variables. The translational velocity $\mathbf{v}_v$ of a large virtual bead modeling the hydrogen-bonded solvent molecule is assumed to be a fast variable in comparison with the corresponding displacement $\mathbf{r}_v$ because of its large mass compared to a methylene or –OH group. Thus, it is valid to neglect the acceleration of the virtual body, i.e., $d\mathbf{v}_v/dt = 0$. The relative motion of the large virtual bead around its relevant equilibrium position is small compared to the dimension of the hydrated volume, since a large fluctuation of the relative position of the virtual body with respect to a frame fixed in the end bead at C^1 would require a drastic increase in the potential energy due to the hydrogen bond linkage. On the basis of these arguments, we set $\mathbf{v}_v = \mathbf{v}_1$. The contracted equation of motion for bead 1 then becomes

$$(m_1 + m_v)\frac{d^2\mathbf{r}_1(t)}{dt^2} = \mathbf{P}_1(t) - \int_0^t dt' \, \xi_{e,1}(t')\mathbf{v}_1(t-t') + \mathbf{R}_{e,1}(t) \tag{III.21}$$

where the effective friction function $\xi_{e,1}(t)$ and the random force $\mathbf{R}_{e,1}(t)$ are $\xi_{e,1}(t) = \xi_1(t) + \xi_v(t)$ and $\mathbf{R}_{e,1}(t) = \mathbf{R}_v(t)$, respectively.

As this study deals in part with the effect of hydrogen bonding on the dynamics of chain motion, the environment of the –OH bead was simulated by incorporating the hydrogen-bonding dynamics into the friction constant $\xi_{e,1}(\chi(t))$ with its dependence on the stochastic variable $\chi(t)$. During the periods when $\chi(t) = 0$, the effective friction function $\xi_{e,1}(t)$ and the random force $\mathbf{R}_{e,1}(t)$ reduce to $\xi_1(t)$ and $\mathbf{R}_1(t)$. Qualitatively, the more hydrogen bonds a solute molecule forms, the greater will be the friction force on the hydrogen-bonded bead. The effective friction coefficient due to hydrogen bonding $\xi_{e,1}$ (as manifested by its effective radius $r_{e,1}$) can be evaluated by calculating the accessible surface area of the solvated volume, calculated from van der Waals increments.[54] This procedure has been found[55] to give quantitative agreement with experimental results for translational and rotational diffusion of protein in aqueous solution. In work on small molecular anions $HCOO^-$ and CH_3COO^- in aqueous solution, the predicted slip viscosity dependence of reorientation times with hydrated volumes agrees very well with experimental measurements.[56]

D. Calculation Procedure. The computer simulations were performed on an IBM RISC system/6000 POWERstation 320. IBM's new superscalar processor is capable of executing four instructions in each machine cycle. The time step used in solving the equations of motion is in the range of $(1-2) \times 10^{-4}$ times the time unit $\tau^* (=\xi_0 b_0^2/kT)$, which is on the order of 10^{-15} s in the temperature range of interest. The total time steps per trajectory are chosen such that the correlation functions of interest have decayed for at least 5 times the correlation times of interest. The ensemble average of the relevant correlation functions is obtained by running 300 trajectories starting from different initial conditions. The total number of time steps in one trajectory run is in the range of 20 000 to 100 000 depending on the temperature used. The initial velocities and dihedral angles are selected from a Boltzmann distribution on the basis of Monte Carlo procedures. A specific number (5000 time steps) of initial simulation runs are discarded to cancel any "memory effect" due to a possible poor choice of initial values for dynamic variables such as friction forces.[36] At the end of each time increment during a trajectory run, the relevant functions of state are stored in arrays to be averaged in the subsequent calculation of correlation functions. Precision in the reported correlation times is estimated to be better than 10% from the reproducibility of the simulations.

In order to calculate the structural relaxation frequency of the solvent, a shear modulus G_∞ is needed. In our recent study[36] of conformational motion in *n*-nonane dissolved in deuterated diglyme, G_∞ was treated as the only adjustable parameter in the GLE simulations and was taken to be independent of temperature. A value of 1.6×10^{10} dyn/cm^2, in reasonable agreement with Fox,[57] was found to best fit the experimental correlation times in nonane. This same value for G_∞ is used in the present GLE simulations of 1-decanol in both deuterated diglyme and ethanol solutions, which uniquely determines the structural relaxation frequency. The absence of internal relaxation modes in methylene chloride allows us to revert to the OLE condition where a delta function is used for the memory function.

Values for p_B, required in the simulations, can be obtained from infrared and NMR spectroscopic data. A plot of $\ln [(1 - p_B(T))/p_b(T)]$ versus $1/T$ then gives a value for ΔH_0, which in turn can be used to evaluate the temperature dependence of the relevant hydrogen bonding rate constants. It is assumed that the hydrogen bond breaking rate constant (k_b) has an Arrhenius-like behavior [i.e., $k_b = A_b \exp(-E_{HB}/kT)$], with two parameters A_b and E_{HB} to be fixed. Since the rate of hydrogen-bond formation is diffusion-controlled with little activation energy, it is assumed that $E_{HB} = \Delta H_0$. By using the experimental values for the dielectric relaxation time τ_D and the diffusion coefficient D_R of 1-decanol, Bertolini et al.[58] obtained $k_b = 0.0067$ ps^{-1} at $T = 298$

(54) Edward, J. T. *J. Chem. Educ.* **1970**, *47*, 261.
(55) Venable, R. M.; Pastor, R. W. *Biopolymers* **1988**, *27*, 1001.
(56) Alms, G. R.; Bauer, D. R.; Brauman, J. I.; Pecora, R. *J. Chem. Phys.* **1973**, *59*, 5321.
(57) Fox, T.; Flory, F. *J. Am. Chem. Soc.* **1948**, *70*, 23; *J. Appl. Phys.* **1950**, *21*, 581; *J. Phys. Chem.* **1951**, *55*, 221; *J. Polym. Sci.* **1954**, *14*, 315.

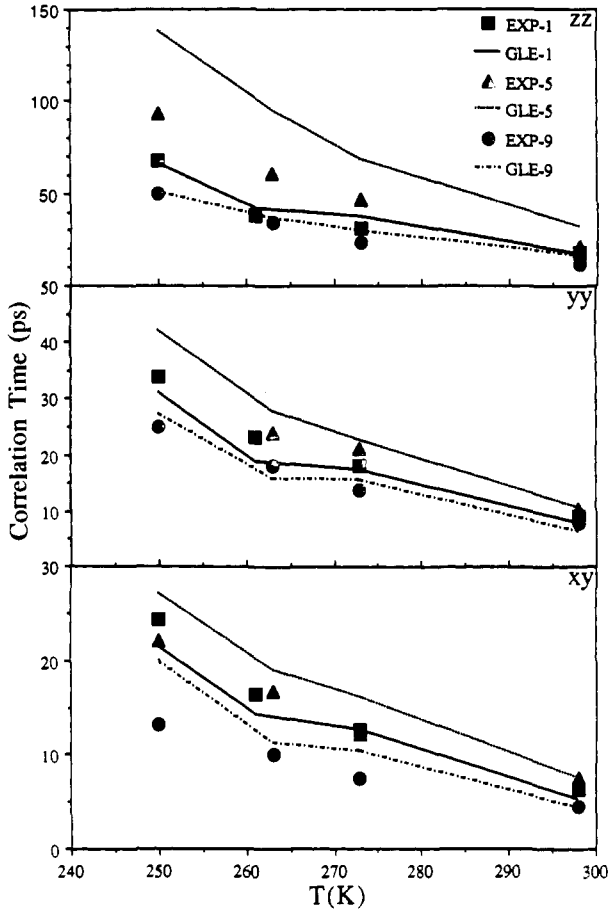

Figure 4. Comparison of the NMR experimental results with the GLE simulations at various temperatures for 1-decanol in deuterated diglyme.

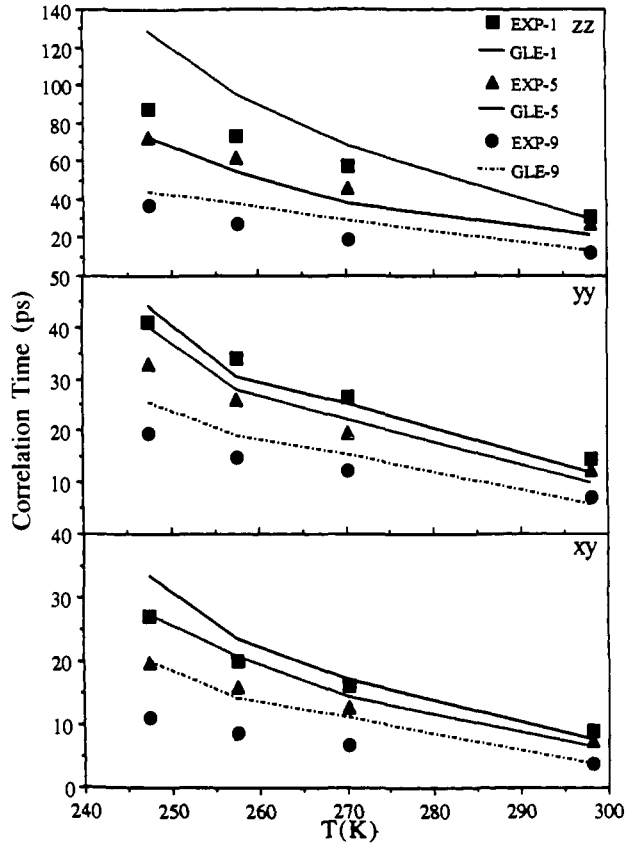

Figure 5. Comparison of the NMR experimental results with the GLE simulations at various temperatures for 1-decanol in deuterated ethanol.

K. The corresponding hydrogen bonding lifetime (τ_{HB} = 150 ps) is much longer than the Cartesian correlation times of 1-decanol for the temperatures of interest. It was found from our test simulations that the calculation results are not sensitive to the hydrogen-bonding lifetime. Thus, the values for k_b derived from the above procedure are used in all the simulations in both deuterated diglyme and ethanol. In deuterated diglyme, the effective radius of the hydrogen bonded –OH group is estimated to be 3.8 Å. Similar but larger changes were introduced for 1-decanol in ethanol (see section IV.C).

IV. Results and Discussion

A. Solvent Relaxation on Chain Motion. The Cartesian correlation times, τ_{xx}, τ_{yy}, τ_{zz}, and τ_{xy}, are calculated at several temperatures from both GLE and OLE simulations. The results for the three labeled positions in 1-decanol dissolved in (1) deuterated diglyme, (2) deuterated ethanol, and (3) deuterated methylene chloride are given along with the experimental values in Tables V–VII. The experimental results along with the best calculations (GLE for diglyme and ethanol solvents and OLE for methylene chloride solvent) also are plotted versus temperature in Figures 4–6. The τ_{xx} was omitted in these figures and in some of the subsequent analysis because these values are relatively poorly determined by the set of NMR experiments.[19] It is noted in Tables V and VI that the GLE simulations in diglyme and ethanol solvents generally give better results than the OLE method in comparison with the experimental results. The shorter correlation times observed in the GLE simulations in comparison with the OLE simulations are apparently due to the reduced effective friction forces in solvents with finite relaxation rates.

Note in Table V or Figure 4 for temperatures greater than 250 K, the GLE simulations with only a structural relaxation mode

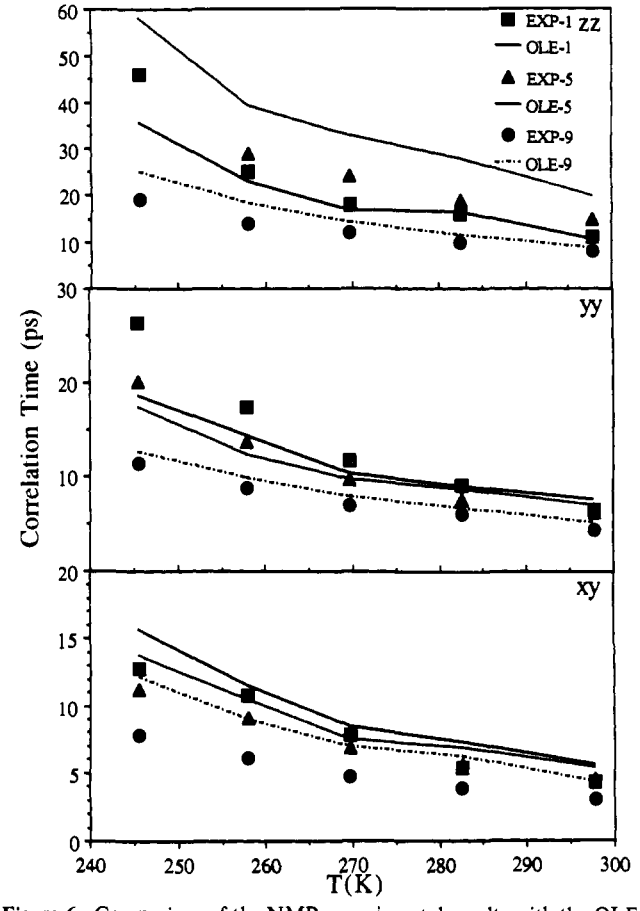

Figure 6. Comparison of the NMR experimental results with the OLE simulations at various temperatures for 1-decanol in deuterated methylene chloride.

(58) Bertolini, D.; Cassettari, M.; Ferrario, M.; Grigolini, P.; Salvetti, G. *Adv. Chem. Phys.* **1985**, *62*, 277.

Table V. Cartesian Correlation Times (ps) of ^{13}C-Labeled (1, 5, and 9 Positions) 1-Decanol in $(CD_3OCD_2CD_2)_2O$

temp, K			C^1	C^5	C^9
298	τ_{xx}	exptl	12 ± 2	12 ± 5	11 ± 2
		GLE[a]	7.3	11.0	6.4
		OLE[b]	15.0	19.2	16.1
	τ_{yy}	exptl	9.1 ± 0.2	10.4 ± 0.9	7.8 ± 0.2
		GLE	7.8	10.8	6.5
		OLE	12.3	19.1	16.3
	τ_{zz}	exptl	18 ± 1	21 ± 3	12 ± 1
		GLE	17.2	31.7	16.0
		OLE	22.4	62.0	27.0
	τ_{xy}	exptl	6.4 ± 0.2	7.6 ± 0.4	4.6 ± 0.2
		GLE	5.4	7.6	4.5
		OLE	11.2	14.3	13.4
273	τ_{xx}	exptl	20 ± 3	20 ± 5	21 ± 4
		GLE	15.6	21.8	13.0
		OLE	32.2	41.6	33.3
	τ_{yy}	exptl	18.0 ± 0.5	21.1 ± 0.7	13.9 ± 0.7
		GLE	17.4	22.7	15.5
		OLE	28.2	40.3	30.8
	τ_{zz}	exptl	31 ± 2	47 ± 3	23 ± 3
		GLE	37.3	68.5	29.6
		OLE	44.6	127	60.2
	τ_{xy}	exptl	12.6 ± 0.3	12.2 ± 0.4	7.4 ± 0.4
		GLE	12.6	16.2	10.4
		OLE	25.8	30.4	25.7
261/263[c]	τ_{xx}	exptl	21 ± 5	32 ± 7	28 ± 4
		GLE	17.4	25.6	13.8
		OLE	42.5	45.4	35.8
	τ_{yy}	exptl	23.2 ± 0.9	24 ± 1	18.2 ± 0.5
		GLE	19.0	27.8	15.7
		OLE	35.5	45.0	35.5
	τ_{zz}	exptl	38 ± 3	61 ± 4	34 ± 3
		GLE	41.9	95.0	36.2
		OLE	53.6	154	64.6
	τ_{xy}	exptl	16.4 ± 0.6	16.8 ± 0.6	10.1 ± 0.4
		GLE	14.3	19.0	11.3
		OLE	34.5	33.2	28.9
250	τ_{xx}	exptl	37 ± 8	40 ± 8	41 ± 5
		GLE	26.3	36.9	23.0
		OLE	60.0	66.3	57.0
	τ_{yy}	exptl	34 ± 1	34 ± 1	24.9 ± 0.9
		GLE	31.1	42.2	27.4
		OLE	47.0	63.2	55.1
	τ_{zz}	exptl	68 ± 5	93 ± 5	50 ± 3
		GLE	65.8	138	50.8
		OLE	71.7	205	102
	τ_{xy}	exptl	24.4 ± 0.9	22.1 ± 0.7	13.3 ± 0.5
		GLE	21.4	27.1	19.9
		OLE	47.8	48.0	46.2

[a] Obtained from the GLE simulations with $G_\infty = 1.6 \times 10^{10}$ dyn/cm^2 and the modified Jorgensen potential for the C–C–C–OH linkage. [b] Obtained from OLE simulations with the modified Jorgensen potential for the C–C–C–OH linkage. [c] The temperatures used for the correlation times are 261 K at C^1 and 263 K at C^5 and C^9.

Table VI. Cartesian Correlation Times (ps) of ^{13}C-Labeled (1, 5, and 9 Positions) 1-Decanol in CD_3CD_2OH

temp, K			C^1	C^5	C^9
298	τ_{xx}	exptl	15 ± 5	13 ± 3	5 ± 2
		GLE[a]	8.4	9.4	5.4
		OLE[b]	18.2	20.2	14.3
	τ_{yy}	exptl	14.6 ± 0.4	12.3 ± 0.5	7.0 ± 0.2
		GLE	11.8	9.7	5.6
		OLE	20.9	20.1	15.0
	τ_{zz}	exptl	31 ± 3	27 ± 2	12 ± 1
		GLE	21.3	29.4	12.8
		OLE	38.7	61.7	26.6
	τ_{xy}	exptl	9.2 ± 0.4	7.6 ± 0.3	3.9 ± 0.2
		GLE	7.7	6.5	3.8
		OLE	16.1	16.1	11.7
270	τ_{xx}	exptl	26 ± 8	22 ± 5	8 ± 3
		GLE	20.0	21.3	14.2
		OLE	35.3	42.4	32.1
	τ_{yy}	exptl	26.4 ± 0.9	19.6 ± 0.7	12.2 ± 0.4
		GLE	25.0	22.0	15.5
		OLE	43.4	40.9	31.3
	τ_{zz}	exptl	57 ± 5	46 ± 3	19 ± 2
		GLE	37.8	67.8	28.8
		OLE	80.0	118	50.8
	τ_{xy}	exptl	16.1 ± 0.8	12.7 ± 0.4	6.9 ± 0.2
		GLE	17.0	14.3	11.2
		OLE	32.9	30.8	26.3
258	τ_{xx}	exptl	33 ± 10	28 ± 5	12 ± 3
		GLE	24.6	29.1	17.9
		OLE	56.2	60.9	47.6
	τ_{yy}	exptl	34 ± 1	26 ± 1	14.8 ± 0.4
		GLE	30.5	28.0	18.9
		OLE	65.1	59.4	49.0
	τ_{zz}	exptl	73 ± 6	62 ± 3	27 ± 2
		GLE	54.4	94.6	37.8
		OLE	114	183	83.3
	τ_{xy}	exptl	20 ± 1	15.8 ± 0.4	8.7 ± 0.3
		GLE	23.3	20.7	14.1
		OLE	51.7	48.2	43.4
248	τ_{xx}	exptl	43 ± 13	32 ± 9	16 ± 3
		GLE	37.6	40.0	25.8
		OLE	72.3	77.1	64.5
	τ_{yy}	exptl	41 ± 2	33 ± 2	19.6 ± 0.5
		GLE	44.1	40.3	25.4
		OLE	82.0	72.3	68.0
	τ_{zz}	exptl	87 ± 8	72 ± 5	37 ± 2
		GLE	71.9	129	43.6
		OLE	137	230	106
	τ_{xy}	exptl	27 ± 1	19.8 ± 0.7	11.2 ± 0.3
		GLE	33.4	27.2	20.0
		OLE	61.2	54.9	53.0

[a] Obtained from the GLE simulations with the modified Jorgensen potential for the C–C–C–OH linkage. [b] Obtained from OLE simulations.

($C_{ss} = 1$) are sufficient in diglyme to yield Cartesian correlation times in good agreement with the experimental values. At lower temperatures (<250 K), however, the deviation between the experimental results and the GLE simulations becomes larger, though improvement over the OLE simulations continues to be evident throughout the relevant temperature range (cf. Table V and VI).

Several factors, ignored in the above analysis, may contribute to these deviations at lower temperatures. One is the influence on the friction force of *slow* relaxation modes. At a low temperature (241 K) and high viscosity about 68% of *both* solute and solvent molecules are now populated in the trans state. The formation of a locally ordered phase would make the cage surrounding the solute molecule sufficiently rigid to significantly "screen" the influence of rapidly fluctuating modes. Thus, slow relaxation modes may make a greater contribution to the frequency-dependent friction force at low temperatures. One possible slow relaxation mode is rotational reorientation of the solvent molecules. At present, the characteristic time and the normalized amplitude C_{rs} for the rotational relaxation in deuterated diglyme are unavailable from the literature. The ratio of relaxation times between the rotational and structural relaxation modes is taken to be 78 in accordance with Sceat's evaluation for *n*-alkane.[59] In Table VIII the calculated correlation times at 241 K are listed as a function of the normalized amplitude C_{rs} for the rotational relaxation mode in the solvent, along with the experimental results for comparison. The simulation results are in good agreement with the experimental values when C_{rs} is set equal to 0.25.

The OLE simulations for 1-decanol in deuterated methylene chloride (cf. Table VII and Figure 6) exhibit good agreement with the experimental values in contrast to the results for 1-decanol in deuterated diglyme and ethanol (cf. Tables V and VI). Methylene chloride is a molecule without internal rotational modes, and motions associated with the structural relaxation modes are either absent or shifted to a faster time domain. In both cases, decay of the correlation between the segmental motion in 1-decanol and the solvent motion becomes fast in comparison with the characteristic times of the motions in the solute. Therefore, the

(59) Cochran, M. A.; Jones, P. B.; North, A. M.; Pethrick, R. A. *J. Chem. Soc., Faraday Trans. 2* **1972**, *68*, 1719.

Table VII. Cartesian Correlation Times (ps) of ^{13}C-Labeled (1, 5, and 9 Positions) 1-Decanol in CD_2Cl_2

temp, K			C^1	C^5	C^9
298	τ_{xx}	exptl	6 ± 2	8 ± 3	4 ± 2
		OLE[a]	5.9	7.0	4.8
	τ_{yy}	exptl	6.5 ± 0.2	6.3 ± 0.4	4.4 ± 0.2
		OLE	7.6	7.0	5.1
	τ_{zz}	exptl	11 ± 1	15 ± 2	8 ± 1
		OLE	10.4	19.9	8.7
	τ_{xy}	exptl	4.3 ± 0.2	4.6 ± 0.2	3.1 ± 0.2
		OLE	5.6	5.4	4.3
283	τ_{xx}	exptl	8 ± 3	10 ± 3	5 ± 2
		OLE	8.1	8.9	7.0
	τ_{yy}	exptl	9.1 ± 0.4	7.6 ± 0.5	6.1 ± 0.2
		OLE	9.0	8.6	6.7
	τ_{zz}	exptl	16 ± 1	19 ± 2	10 ± 1
		OLE	16.5	27.9	11.4
	τ_{xy}	exptl	5.4 ± 0.3	5.6 ± 0.2	3.9 ± 0.2
		OLE	7.3	6.9	6.3
270	τ_{xx}	exptl	8 ± 3	12 ± 3	6 ± 2
		OLE	8.3	10.2	8.5
	τ_{yy}	exptl	11.8 ± 0.4	9.7 ± 0.4	7.0 ± 0.2
		OLE	10.3	9.8	7.9
	τ_{zz}	exptl	18 ± 2	24 ± 2	12 ± 1
		OLE	16.8	32.9	14.2
	τ_{xy}	exptl	7.8 ± 0.2	6.9 ± 0.2	4.8 ± 0.2
		OLE	8.5	7.6	7.0
258	τ_{xx}	exptl	12 ± 3	14 ± 3	7 ± 3
		OLE	11.1	12.7	10.5
	τ_{yy}	exptl	17.3 ± 0.5	13.7 ± 0.5	8.9 ± 0.4
		OLE	14.3	12.4	9.9
	τ_{zz}	exptl	25 ± 2	29 ± 2	14 ± 2
		OLE	22.8	39.3	18.4
	τ_{xy}	exptl	10.8 ± 0.3	9.1 ± 0.3	6.1 ± 0.3
		OLE	11.5	10.5	9.0
246	τ_{xx}	exptl	17 ± 5	20 ± 4	10 ± 3
		OLE	15.8	17.6	14.5
	τ_{yy}	exptl	26.4 ± 0.7	20.1 ± 0.7	11.4 ± 0.4
		OLE	18.6	17.4	12.7
	τ_{zz}	exptl	46 ± 3	46 ± 2	19 ± 2
		OLE	35.7	58.2	25.1
	τ_{xy}	exptl	12.8 ± 0.4	11.2 ± 0.3	7.8 ± 0.3
		OLE	15.9	13.8	12.2

[a] Obtained from the OLE simulations with the modified Jorgensen potential for the C–C–C–OH linkage.

Table VIII. Cartesian Correlation Times (ps) of ^{13}C-Labeled (1, 5, and 9 Positions) 1-Decanol in $(CD_3OCD_2CD_2)_2O$ at 241 K, Simulated from GLEs with Different C_{rs} and OLEs, Along with the Experimental Results

C_{rs}	τ_{xx}	τ_{yy}	τ_{zz}	τ_{xy}
0.0	74.6 (1)[a]	64.0	90.8	60.8
	72.9 (5)	70.8	187	54.3
	59.4 (9)	59.2	95.9	51.6
0.10	47.9	44.9	89.5	36.5
	52.4	51.3	179	34.5
	42.9	39.0	78.7	32.0
0.25	44.1	41.1	80.1	34.6
	44.9	43.7	164	29.7
	34.7	34.1	72.1	25.8
exptl	39 ± 8	38 ± 1	72 ± 5	28.7 ± 0.9
	50 ± 10	47 ± 2	108 ± 6	28.7 ± 0.9
	36 ± 7	31 ± 1	56 ± 4	17.6 ± 0.6
OLE[b]	92.3	84.4	183	69.6
	104	95.6	300	74.4
	89.4	86.6	151	64.6

[a] The number in parentheses denotes the carbon position in 1-decanol. [b] Obtained from the OLE simulations.

OLEs with a δ-memory kernel is capable of providing a satisfactory description of 1-decanol in methylene chloride.

If only overall molecular motion contributes to the relaxation of the local modes, Cartesian correlation times at different chain positions should remain the same. As suggested in Tables V–VII, however, the inequality relation

$$\tau(C^5) > \tau(C^1) > \tau(C^9)$$

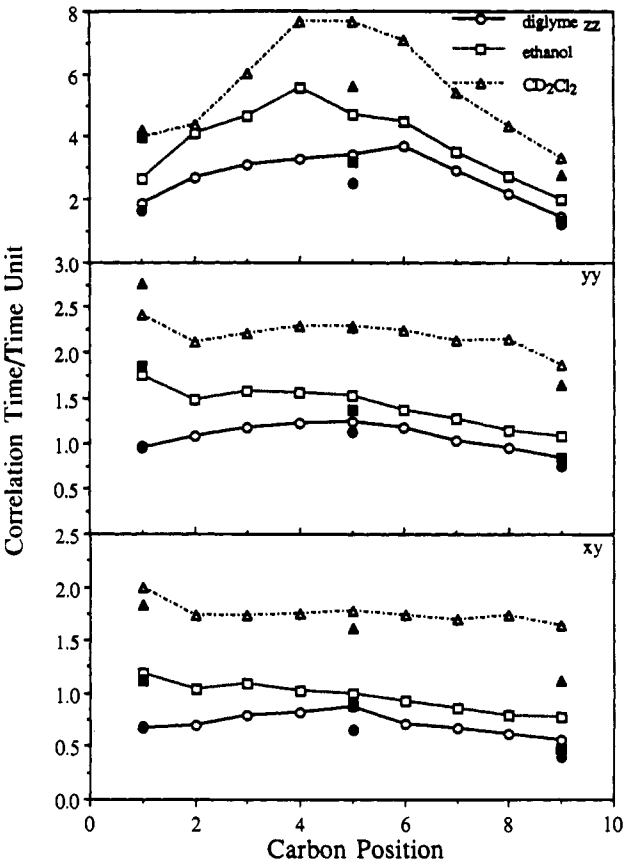

Figure 7. Reduced Cartesian correlation times for the *zz*, *yy*, and *xy* modes vs carbon positions. Solid symbols represent experimental results and open symbols represent calculated results.

exists for most of the Cartesian modes except some in the ethanol solvent where extensive hydrogen bonding at the –OH group may more firmly anchor the $^{13}CH_2$ (C^1) group resulting in significant changes in the correlation times for certain Cartesian modes. For the motion of hydrocarbon chains in solution, two factors should be considered in rate-determining processes. One is the barrier to isomerization transitions and the other is the friction force exerted by the surrounding solvent. The greater the amount of solvent volume which must be excluded due to the motion of the solute molecule, the larger the friction force exerted on the molecule will be. On the basis of this argument, the smaller group (either –OH or $-CH_3$) attached at C^1 or C^9, respectively, can reorient relatively easier than the longer chain segments attached to C^5. The above experimental results are consistent with this intuitive steric concept, although the relative importance of the steric effect verses the hydrogen-bond anchoring effect requires experimental information to quantify the steric intuition.

Figure 7 shows the reduced Cartesian correlation times in different solvents as a function of carbon positions. The reduced correlation times τ_q (q = *xx*, *yy*, *zz*, *xy*) are defined as τ_q/τ^*, where τ^* is the time unit. The difference in the reduced Cartesian correlation times at the *same* bead in different solvents is obviously a result of both hydrogen bonding at C^1 and coupling of relaxation between the designated bead and its surrounding solvent. A comparison of the correlation times in diglyme and ethanol solvents indicates that the anchoring effect of hydrogen bonding at C^1 falls off with distance from the hydrogen bonding center. Therefore, it has a minimum impact on the motion of the segment at the other end of the molecule compared with its impact on more proximate beads. Thus, the relaxation dynamics of the Cartesian modes at the C^9 position may be utilized to further analyze the effect of finite relaxation frequency on the segmental motion of 1-decanol in solutions. The OLE method, as suggested by our OLE simulations, predicts that the reduced correlation times are invariant in different solvents. However, referring to Figure 7, the reduced correlation times for the Cartesian modes *xy*, *yy*, *zz* at the C^9

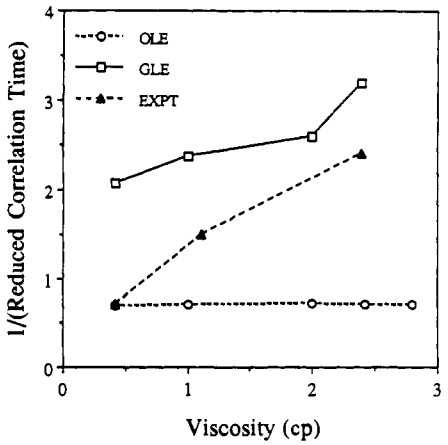

Figure 8. Reciprocals of reduced correlation times for the *xy* mode at C^9, obtained from the experiments, the GLE simulations, and the OLE simulations, vs viscosity.

Table IX. Apparent Activation Energies (kcal/mol) for the Cartesian Modes and End-to-End Direction of 1-Decanol in Diglyme[a]

carbon position	*xx*	*yy*	*zz*	*xy*	end-to-end
					1.1 (0.4)
1	2.0 (0.2)[b]	1.6 (0.3)	1.7 (0.4)	1.7 (0.5)	
5	1.3 (0.2)	1.2 (0.2)	1.2 (0.2)	1.3 (0.3)	
9	2.3 (0.2)	2.1 (0.2)	2.0 (0.2)	2.5 (0.4)	

[a] The solvent viscosity is fixed at a constant η = 2.39 cP. [b] The value in parentheses is one standard deviation.

position in methylene chloride are about twice as large as those in diglyme. A Cartesian mode in a higher viscosity solvent tends to have smaller reduced correlation times. This result can be embodied in an empirical relation

$$\tau^{-1} = A/\eta^{\alpha} \qquad \text{(IV.1)}$$

In Figure 8, the reciprocals of the experimental reduced correlation times for the fastest mode *xy* at C^9 are plotted together with both GLE and OLE simulations. The *xy* mode is influenced most by the local torsional motions as suggested from the apparent energy data in Table IX and is affected least by hydrogen bonding at the other end of the molecule. A least-squares fit of the GLE simulation results gives a value for the exponent, α = 0.5, significantly less than unity. In accordance with Kramer's theory, a value of $\alpha \approx 1$ is obtained for the data from the OLE simulations. The fractional viscosity relationship, eq IV.1 has been found in many physical systems where the diffusing particle has a dimension smaller than the solvent molecules. For instance, a recent study of diffusion of xenon in liquid alkanes[60] has shown that the diffusion coefficient for xenon was proportional to $\eta^{-\alpha}$ with α equal to 0.71 rather than 1 as predicted by the Stokes–Einstein relation. Our simulations suggest that this fractional viscosity dependence results from the dynamic memory effect and is significant in explaining the experimental results.

B. Torsional Potential for Hydroxyl Bead. The effect of C^3–C^2–C^1–OH torsional potentials can be appreciated best in methylene chloride and at higher temperature where the effect of hydrogen bond anchoring at C^1 is diminished. From Table VII it is apparent that the experimental values are not symmetric about the chain center (C^5). The mobility at the position C^9 is generally higher than at the C^1 end. One possible cause of this asymmetry is the difference between the trans–gauche transition barriers in the –C–C–C–OH and –C–C–C–C linkages with the former being 3.07 kcal/mol in the modified Jorgensen potential (cf. eq III.14) and the latter 2.95 kcal/mol in the R–B potential (cf. eq III.12). This variation in transition barriers alone increases the Cartesian correlation times at C^1 by a factor of 1.22 over that at C^9.

The Cartesian modes *yy* and *xy* at C^1 in methylene chloride have correlation times even longer than the corresponding modes at the central bead C^5. This result suggests a preference for populating the –C–C–C–OH linkage more in gauche states than found in the –C–C–C–C linkages. Both *yy* and *xy* modes in gauche states have greater projections on the major axis of the chain and the dominant relaxation mechanism for these two modes is via rotation around the major axis of the chain.[36] Modifying Jorgensen's 1-propanol potential by reducing the trans–gauche energy gap to 0.0 kcal/mol resulted in improved agreement between simulational and experimental results (cf. Table VII and Figure 6).

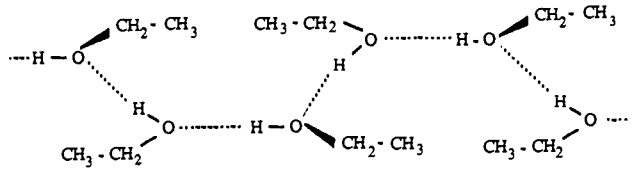

Figure 9. A schematic depiction of hydrogen network in ethanol solvent.

C. Hydrogen Bond Anchoring Effects. The effect of hydrogen bond anchoring on segmental motion in 1-decanol can be analyzed by referring to Figure 7. In Figure 7 the extent of the asymmetry about C^5 in correlation time plots varies with the solvents used and is most pronounced in ethanol. The greater anchoring effect of hydrogen bonding in the highly associated ethanol may be due to two factors. First, ethanol is a hydrogen-bond donor as well as a hydrogen-bond acceptor allowing up to three (two acceptors and one donor) hydrogen bonds between ethanol and 1-decanol. The second, and more likely, factor is the extended network of hydrogen bonds which may form in ethanol between solvent molecules themselves. A possible chain model, adopted from the solid and simplified for the liquid, is illustrated in Figure 9.

Some branching of chains is possible and the presence of small hydrogen-bonded oligomers is supported by infrared studies on liquid ethanol.[61] A Monte Carlo simulation of liquid ethanol at 25 °C by Jorgensen[62] gives the percentage of ethanol monomers with 0, 1, 2, and 3 hydrogen bonds as 4, 29, 56, and 11, respectively. From the ratio of monomers with one and two hydrogen bonds, an average chain length of five to six monomers is estimated. Oligomers with even larger chain lengths would be expected if monomers involve three hydrogen bonds. An effective friction constant for the hydrogen-bonded bead is thus used to characterize this three-dimensional structure in ethanol. An adjustable friction parameter in the present GLE simulations avoids analytical solutions that are essentially intractable. Should the hydrogen bond network in ethanol "ice up" several beads at the –OH end of the molecule, the solvent would impose higher friction forces upon several beads near the –OH end. Satisfactory results are obtained in Table VI by increasing, in an ad hoc manner, the friction constant for the beads –OH, C^1, and C^2 by factors of 5, 3, and 1, respectively, times that of the central bead C^5.

D. Temperature Dependence at a Fixed Viscosity. In contrast to motion in a vacuum, the various temperature-dependent modes in 1-decanol are due partly to the viscosity of the solvent. If the internal motion (i.e., isomerization transitions) dominates over the overall rotation for the relaxation processes, the remaining temperature dependence is Arrhenius-like with an activation energy roughly equal to the barrier height between the trans and gauche states. The trans–gauche barrier is 2.95 kcal/mol for the R–B torsional potential, much larger than the thermal energy *kT*. While holding the zero-frequency viscosity fixed along with other parameters in the deuterated diglyme, one can vary temperature to determine an apparent activation energy arising from contributions other than solvent viscosity. The apparent activation energies for 1-decanol at a fixed shear viscosity η = 2.39 cP are

(60) Pollack, G. L.; Kennan, R. P.; Himm, J. F.; Stump, D. R. *J. Chem. Phys.* **1990**, *92*, 625.

(61) Luck, W. A. P.; Ditter, W. *Ber. Bunsen-Ges. Phys. Chem.* **1968**, *72*, 365.

(62) Jorgensen, W. L. *J. Am. Chem. Soc.* **1981**, *103*, 345.

listed in Table IX. In this exercise, the reorientation of the end-to-end direction with the longest correlation time exhibits the lowest apparent activation energy, while the *xy* mode with the shortest correlation times at C^9 experiences the largest apparent activation energy. The lower apparent activation energy at C^1 versus C^9 is in an opposite direction to the trans–gauche transition barriers of the linkages –C–C–C–OH versus –C–C–C–C. This depression of the internal torsional motion in the –C–C–C–OH linkage reflects the effect of solvation due to hydrogen bonding in the –OH group.

The apparent activation energies for the Cartesian modes at the C^1 and C^9 beads are always larger than the corresponding modes at the central bead suggesting that proportionally more isomerization transitions are involved in relaxing the Cartesian modes at the outer beads than near the central beads. This is in accordance with the physical intuition that torsional motion of end bonds can be realized by the swing of small terminal groups requiring motion through only a relatively small amount of solvent volume. Motion about the bonds near the center of the chain requires swings of the attached groups through large volumes thereby imposing considerable friction force. Cooperative motion of proximate bonds such as the formation of kinks and jogs, as in the crankshaft rotational model,[63] can reduce the motion of long tails, but such cooperative motions also would require an activation energy of approximately one barrier height.[64] As the apparent activation energies for the Cartesian modes appear to be reduced at the central bead, it is concluded for the molecular size of 1-decanol that cooperative transitions have only a minor effect on the segmental motion near the chain's center. It is concluded, therefore, for the 1-decanol that the overall rotation of the molecule is a significant mechanism for spin relaxation in the chain center. Cooperative motion offers the only feasible mode of relaxation in long chain polymer systems.

V. Conclusion

In summary, the isotopic decanols carbon-13 labeled at 1, 5, and 9 positions have been synthesized and the relaxation of different magnetization modes in this molecule has been measured via carbon-13 NMR coupled relaxation techniques. The combined application of different pulse preparations including a new *J*-pulse perturbation leads to more reliable relaxation results. Not only is the overall fitting accuracy improved, but some correlations between the experimental spectral densities are also reduced. The correlation times τ_{xx}, τ_{yy}, τ_{zz}, and τ_{xy} for different molecular directions have been obtained from the dipolar spectral densities. By comparing the correlation times for the $^{13}CH_2$ moiety at different positions and in different solvents, it is concluded that the formation of a hydrogen bond between 1-decanol and the solvents such as diglyme and ethanol has a significant effect on the motion of nearby chain segments and the anchoring effect in ethanol is considerably more than that in diglyme. Nevertheless, the hydrogen bond anchor is less effective in controlling the magnitude and anisotropy of chain motion than the bulk effect associated with the two chain segments at C^5 in decanol. These studies, because of the "richness" of data, indicate the high promise of NMR multiplet spin relaxation data in producing the motional details of flexible paraffin chains.

This stochastic dynamics study of 1-decanol in various solutions indicates the importance of a memory function in Langevin equations to describe both global and segmental motions of chain molecules in solvents with structural relaxation modes. Nevertheless, OLEs can provide a satisfactory description of the solute relaxation in solvents like methylene chloride without relaxation modes capable of coupling efficiently with the flexible solute chain. In diglyme and ethanol for temperatures greater than 250 K, a GLE hydrodynamic description with structural relaxation modes in the solvents and with the slip boundary condition yields Cartesian correlation times that agree better with the NMR coupled relaxation experiments. At lower temperatures (<250 K) the introduction of slow solvent relaxation modes (e.g., rotational relaxation) brings dynamic simulations in even closer agreement with the experiments.

By comparison of simulations with the NMR experimental data, it is found that a better fit of the experimental data can be realized with a modified Jorgensen torsional potential for the –C–C–C–OH linkage, which gives more preference to gauche states. As the Jorgensen torsional potential was derived for 1-propanol, one may expect variations in 1-decanol due to differential solvent packing effects. Another interesting result emerging from the present study is that hydrogen bonding in an associated solution may exhibit an even greater anchoring effect not only on the hydrogen bonded bead itself but also on adjacent beads due to an extended network of solvent hydrogen bonds. Variations in the relaxation parameters for 1-decanol in diglyme and ethanol would appear to be best explained by the extent of hydrogen bond dissociation.

Acknowledgment. We thank Professor Glenn T. Evans for stimulating discussions. This work was supported in part by the National Institute of General Medicine Science of the National Institutes of Health under Grant No. GM 08521-30.

Appendix

A. Preparation of 1-Decanol-*1*-^{13}C.

$$n\text{-}C_9H_{19}Cl \xrightarrow{Na^{13}CN} n\text{-}C_9H_{19}{}^{13}CN \xrightarrow{H_2O/H^+} n\text{-}C_9H_{19}{}^{13}COOH \xrightarrow{LiAlH_4/THF} n\text{-}C_9H_{19}{}^{13}CH_2OH$$

Decanitrile.[65] 1-Chlorononane (2.44 g, Aldrich) was added to a stirred solution of sodium cyanide ($Na^{13}CN$, 0.78 g) in dimethyl sulfoxide (3 mL) at 80 °C. The solution was then heated at 140 °C for 15 min. The reaction solution was cooled, diluted with saturated brine (50 mL), extracted with ether, and dried over sodium sulfate. Distillation gave 2.4 g, 15.68 mmol, 100%, and bp 108–125 °C (22 mm).

***n*-Decanoic Acid-*1*-^{13}C.** A magnetically stirred solution of decanonitrile (2.4 g) in glacial acetic acid (2.5 mL), water (2.5 mL), and concentrated sulfuric acid (2.5 mL) was refluxed for 22 h. The reaction mixture was diluted with water (40 mL), and extracted with benzene. The combined organic phases were washed with saturated brine, dried, and distilled to obtain *n*-decanoic acid (2.48 g, 91.9%): bp 95–105 °C (0.2 mm), lit.[66] 270 °C (atmospheric pressure).

1-Decanol-*1*-^{13}C. A solution of *n*-decanoic acid (2.48 g) in 18 mL of anhydrous tetrahydrofuran was added to a stirred slurry of lithium aluminium hydride (0.31 g, in THF, 12 mL) while cooling in an ice water bath. After the mixture was stirred for 10 h at room temperature, the excess lithium aluminum hydride was decomposed by treatment with concentrated hydrochloric acid (2.6 mL) and then with water (2.6 mL). The reaction mixture was extracted with ether and the extracts were washed with saturated brine and dried over sodium sulfate. The product, 1-decanol-*1*-^{13}C, was obtained in 85.7% yield (1.12 g, 7.07 mmol), bp 128–133 °C (20 mm). The compound was shown to be pure by ^1H and ^{13}C NMR.

B. Preparation 1-Decanol-*5*-^{13}C.

$$HO\text{–}(CH_2)_4\text{–}OH \xrightarrow{Na/CH_3I} CH_3O\text{–}(CH_2)_4\text{–}OH \xrightarrow{SOCl_2/Py} CH_3O\text{–}(CH_2)_4\text{–}Cl \xrightarrow{Na^{13}CN} CH_3O(CH_2)_4{}^{13}CN \xrightarrow{C_5H_{11}Li/Et_2O} CH_3O\text{–}(CH_2)_4\text{–}{}^{13}C(=O)\text{–}C_5H_{11} \xrightarrow{LiAlH_4/THF} CH_3O\text{–}(CH_2)_4{}^{13}CH(OH)\text{–}C_5H_{11} \xrightarrow{CH_3SO_2Cl/Py} CH_3O\text{–}(CH_2)_4{}^{13}CH(OSO_2CH_3)\text{–}C_5H_{11} \xrightarrow{LiAlH_4/THF} CH_3O\text{–}(CH_2)_4{}^{13}CH_2\text{–}C_5H_{11} \xrightarrow{NaI + (CH_3)_3CC(=O)Cl} (CH_3)_3CC(=O)O(CH_2)_4{}^{13}CH_2\text{–}C_5H_{11} \xrightarrow{LiAlH_4/THF} C_5H_{11}\text{–}{}^{13}CH_2(CH_2)_4\text{–}OH$$

(63) Skolnick, J.; Helfand, E. *J. Chem. Phys.* **1980**, *72*, 5489.
(64) Helfand, E. *Science* **1985**, *226*, 647.
(65) Smiley, R. A.; Arnold, C. J. *J. Org. Chem.* **1960**, *25*, 257.
(66) Kabalka, G. W.; Kunda, S. A.; Kunda, U. S.; Delgado, M. C. *J. Org. Chem.* **1984**, *49*, 174.

4-Hydroxybutyl Methyl Ether. To a solution of 1,4-butanediol (70 g, 0.778 mmol, Aldrich) in dry toluene (20 mL) at 88–105 °C (internal) was added sodium (5 g, 0.217 g-atom) in small pieces. The reaction mixture was heated at reflux temperature until all sodium dissolved and iodomethane (15 mL) was added slowly at 105 °C. After the mixture was refluxed for 2 h, toluene was distilled out and the product, 4-hydroxybutyl methyl ether, was obtained in 76.8% yield (17.36 g, 16.7 mmol): bp 108–118 °C, lit.[67] 66 °C (7 mm). This was pure by ^{13}C NMR.

4-Chlorobutyl Methyl Ether. A solution of 6.0 g of the above alcohol and 5.6 mL of dry pyridine was chilled to 10 °C and 6.3 mL of thionyl chloride was added dropwise at such a rate that the temperature was maintained between 10 and 30 °C. After the addition of thionyl chloride, the reaction mixture was heated for 3 h on a steam bath. The solution was chilled, poured onto ice, and extracted with ether and the combined ether extracts were washed with saturated brine. After drying over sodium sulfate, 4-chlorobutyl methyl ether was obtained in 75.0% yield (5.30 g, 43.3 mmol): bp 130–137 °C, lit.[68] 142.5–142.8 °C (751 mm).

5-Methoxypentanonitrile-*1*-^{13}C. 4-Chlorobutyl methyl ether (4.64 g) in 9.5 mL of anhydrous dimethyl sulfoxide was added in 20 min to a stirred mixture of sodium cyanide-^{13}C (1.98 g) in DMSO (11.4 mL) at 80 °C. The reaction was exothermic. The mixture was heated at 140–145 °C for 30 min. The resulting yellow mixture was cooled, diluted with saturated brine (50 mL) and worked up as described in the preceding experiment to give 5-methoxypentanonitrile-*1*-^{13}C (3.81 g, 33.7 mmol, 89.0%), bp 83–86 °C (12 mm). The reported natural-abundance material boils at 80–81 °C (15 mm).[69]

Preparation of *n*-Pentyllithium.[70] A 200-mL three-neck flask was equipped with a magnetic stirrer (sealed in glass), a low temperature thermometer, and a dropping funnel. After the apparatus was swept with dry argon, 2.18 g (0.34 g-atom) of lithium wire, wound in a loose coil, rinsed with petroleum ether, and flattened, was cut into pieces about 7 mm in length which fell directly into the reaction flask in a stream of argon. Fifty milliliters of anhydrous ether was added to the flask. With the stirrer started, about 12 drops of a solution of 19.1 g of 1-bromopentane in 25 mL of dry ether was added from a dropping funnel and the reaction mixture was then cooled to −10 °C with a dry ice–2-propanol bath. The remainder of the 1-bromopentane was then added at an even rate over a 30-min period. After the addition was complete, the reaction mixture was allowed to warm to 0–10 °C while stirring for 2 h.

1-Methoxy-5-decanone-*5*-^{13}C. A dry 500-mL three-neck flask fitted with a filtering funnel (with a stopcock) was flushed with argon and the 5-methoxypentanonitrile (3.81 g, 33.7 mmol) was added in 180 mL of anhydrous ether. The magnetically stirred solution was cooled in an ice water bath and the pentyllithium prepared above was introduced dropwise over 10 min. After the addition, the light yellow reaction mixture was refluxed for 4 h and cooled. Part of a solution of 260 g of ammonium chloride in 688 mL of water was added. The remainder of the ammonium chloride was added to the reaction mixture while transferring to a separation funnel. The aqueous phase was extracted twice with ether and the combined ethereal extracts were washed with saturated brine and dried over anhydrous sodium sulfate. Distillation gave the product (4.11 g, 22.1 mmol, 65.5%), bp 134–138 °C (0.3 mm).

Methyl 5-Hydroxydecyl-*5*-^{13}C Ether. A solution of methyl 5-oxodecyl ether (4.11 g) in anhydrous tetrahydrofuran (40 mL) was added to a slurry of lithium aluminum hydride (0.84 g) in dry THF (41 mL) while cooling in an ice water bath. After the mixture was stirred for about 12 h at room temperature, the excess lithium aluminum hydride was hydrolyzed with water (10.6 mL) and then with concentrated hydrochloric acid (10.6 mL). The solution was extracted with ether and the extracts were washed with sodium bicarbonate (8%) and then with saturated brine and dried over sodium sulfate. The residue after removal of the solvent was used directly in the next step.

The Mesylate of the above Compound.[71] The above alcohol in 10.6 mL of pyridine was added with stirring to a solution of freshly redistilled methanesulfonyl chloride (11.74 g) in 4.2 mL of anhydrous pyridine at 0 °C. During the 3.5-h period, additional pyridine (five 10.6-mL portions) was added to the mixture (one addition every 30 min) at 0 °C after which it was allowed to warm to room temperature with stirring for a 12-h period. The reaction mixture was poured onto ice and extracted with ether. The extracts were washed successively with ice water, 1 N hydrochloric acid, saturated sodium bicarbonate, water, and saturated brine. The solvent was removed from the dried (Na_2SO_4) extract and the residue reduced directly.

Methyl Decyl-*5*-^{13}C Ether.[71] The above mesylate in 9.5 mL of THF was added to a stirred slurry of lithium aluminum hydride (7.21 g) in 54 mL of anhydrous THF while chilling in an ice water bath and the reaction mixture was refluxed for 5 h. After hydrolysis with water (136 mL) and addition of concentrated hydrochloric acid (95 mL), the organic phase was separated, the aqueous phase was extracted with ether, and the combined extracts were washed with saturated brine and dried over sodium sulfate. The product, methyl decyl-*5*-^{13}C ether was obtained in 81.8% yield (3.11 g, 18.1 mmol), bp 109–112 °C (13 mm).

Decyl-*5*-^{13}C Trimethylacetate.[72] To an acetonitrile (4.5 mL) solution of methyl decyl ether (3.11 g) and sodium iodide (3.98 g) was added an acetonitrile (4.5 mL) solution of pivaloyl chloride (3.15 g) at 0 °C. After the mixture was stirred at room temperature for 24 h, the reaction was quenched by the addition of aqueous $NaHSO_3$. After extraction with ether followed by drying over anhydrous sodium sulfate, distillation of the solution gave the product, decyl-*5*-^{13}C trimethylacetate (3.99 g, 16.5 mmol, 81.2%), bp 145–148 °C (14 mm).

1-Decanol-*5*-^{13}C. The above acetate (3.99 g) in THF (30 mL) was added slowly with cooling (ice water bath) to a mixture of 37 mL of THF and 0.87 g of lithium aluminum hydride. After stirring for 12 h at room temperature, the reaction mixture was hydrolyzed with water (7.4 mL) and concentrated hydrochloric acid (7.4 mL) and then extracted with ether. The combined organic phases were washed with saturated brine and dried over anhydrous sodium sulfate. The product, 1-decanol-*5*-^{13}C, obtained in 93.1% yield (2.43 g, 15.4 mmol), boiled at 118–121 °C (14 mm). This compound had the correct structure with only a very small amount of impurity as shown by ^{13}C and ^1H NMR.

C. Preparation of 1-Decanol-*9*-^{13}C.

$$HO\text{–}(CH_2)_8\text{–}OH \xrightarrow{HBr/C_6H_{12}} Br\text{–}(CH_2)_8\text{–}OH \xrightarrow{CH_3OH/Na}$$

$$CH_3O\text{–}(CH_2)_8\text{–}OH \xrightarrow{SOCl_2/Py} CH_3O\text{–}(CH_2)_8\text{–}Cl \xrightarrow{Na^{13}CN}$$

$$CH_3O\text{–}(CH_2)_8\text{–}{}^{13}CN \xrightarrow{CH_3Li/Et_2O}$$

$$CH_3O\text{–}(CH_2)_8{}^{13}C(=O)\text{–}CH_3 \xrightarrow{LiAlH_4/THF}$$

$$CH_3O\text{–}(CH_2)_8{}^{13}CH(OH)\text{–}CH_3 \xrightarrow{CH_3SO_2Cl/Py}$$

$$CH_3O\text{–}(CH_2)_8{}^{13}CH(OSO_2CH_3)\text{–}CH_3 \xrightarrow{LiAlH_4/THF}$$

$$CH_3O\text{–}(CH_2)_8{}^{13}CH_2CH_3 \xrightarrow{NaI + (CH_3)_3CC(=O)\text{–}Cl}$$

$$(CH_3)_3CC(=O)\text{–}O(CH_2)_8{}^{13}CH_2\text{–}CH_3 \xrightarrow{LiAlH_4/THF}$$

$$CH_3{}^{13}CH_2\text{–}(CH_2)_8\text{–}OH$$

8-Bromo-1-octanol. A solution of 1,8-octanediol (6.0 g) and hydrobromic acid (48%, 185 mL) plus water (57 mL) was put in a continuous extractor. The extractor was heated to 75 °C in a glycerol bath and cyclohexane was passed through continuously for 60 h. The cyclohexane layer was separated, concentrated, and

(67) Pchat, L.; Baret, C.; Audinot, M. *Bull. Soc. Chim. Fr.* **1965**, 151.
(68) Palomar, M. H.; Jansson, R. *Ber. Dtsch. Chem. Ges.* **1931**, *64*, 1608.
(69) Kirrmann, A.; Geiger-Berschandy, S. *Bull. Soc. Chim. Fr.* **1956**, 991.
(70) Gilman, H.; Beel, J. A.; Bullock, M. W.; Dunn, G. E.; Mill, L. S. *J. Am. Chem. Soc.* **1949**, *71*, 1499.
(71) Peter, H.; Archer, B. A.; Mosher, H. S. *J. Org. Chem.* **1967**, *32*, 1382.
(72) Oku, A.; Harada, T.; Kita, K. *Tetrahedron Lett.* **1982**, *23*, 681.

then dried over anhydrous potassium carbonate. The product was obtained in 97.3% yield (8.37 g): bp 106–108 °C (0.4 mm), lit.[73] bp 81 °C (0.06 mm).

8-Methoxy-1-octanol. To a solution of 0.91 g of sodium in 45 mL of anhydrous methanol was added a solution of 7.65 g of 8-bromo-1-octanol in 27 mL of methanol. The mixture was then refluxed for 23 h. The methanol was evaporated and the residue was diluted with water, the aqueous layer was extracted with ether, and the combined extracts were washed with saturated brine and dried over sodium sulfate. Distillation gave 5.51 g, 34.4 mmol, 94.1%, and bp 128–133 °C (15 mm).

8-Chlorooctyl Methyl Ether. A solution of 8-methoxy-1-octanol (5.51 g) in anhydrous pyridine (3.7 mL) was chilled in an ice water bath. Thionyl chloride (4.3 mL) was added dropwise at such a rate that the internal temperature was maintained at 10–30 °C. After the addition, the reaction mixture was heated on the steam bath for 3 h. The mixture was then cooled and poured onto ice. The product was extracted into ether and the ether extracts were washed and dried. The product was obtained in 83.6% yield (5.14 g, 28.8 mmol), bp 110–114 °C (15 mm). The structure of this compound was correct and quite pure as shown by ^{13}C NMR.

9-Methoxynonanonitrile-*1*-^{13}C. 8-Chlorooctyl methyl ether (5.14 g) in anhydrous dimethyl sulfoxide (DMSO, 7.2 mL) was added to a stirred mixture of sodium cyanide (99% ^{13}C, 1.5 g) in DMSO (8.8 mL) at 80 °C. The reaction mixture was heated at 140 °C for 20 min. After the mixture had cooled, saturated brine (25 mL) was introduced, and the product was extracted into ether and dried. The product was obtained in 94.4% yield (4.60 g, 27.2 mmol), bp 138–144 °C (16 mm).

10-Methoxy-2-decanone-*2*-^{13}C. To a solution of 9-methoxynonanonitrile (4.60 g) in anhydrous ether (230 mL) was added via syringe a solution of methyllithium in ether (1.57 M, 54 mL) while cooling in an ice water bath. The reaction mixture was then refluxed for 4 h. After the mixture had cooled, a solution of ammonium chloride (170 g in 460 mL of water) was introduced and the product was extracted into ether and dried. The product was obtained in 76.0% yield (3.86 g, 20.7 mmol) bp 80 °C (0.14 mm).

10-Methoxy-2-decanol-*2*-^{13}C. A solution of 10-methoxy-2-decanone-*2*-^{13}C (3.86 g) in dry THF (40 mL) was added to a slurry of lithium aluminum hydride (0.80 g) in THF (40 mL) while cooling in an ice water bath. After stirring at room temperature for 12 h, the excess lithium aluminum hydride was hydrolyzed by adding water (10 mL) and concentrated hydrochloric acid (10 mL). The reaction mixture was extracted with ether and the combined organic phases were washed with saturated sodium bicarbonate and saturated brine and then dried (Na_2SO_4). The solvent was removed and the residue used in the next step.

The Mesylate of the above Product. The above alcohol in 10.0 mL of pyridine was added with stirring to a solution of freshly distilled methanesulfonyl chloride (11.0 g) in 4.0 mL of anhydrous pyridine at 0 °C. During the 3.5-h period, additional pyridine (five 10.0-mL portions) was added to the mixture (one addition every 30 min) at 0 °C. After the addition, the reaction mixture was poured into ice water and the aqueous part was extracted with ether. The combined ether extracts were washed successively with ice water, hydrochloric acid (1 N), saturated sodium bicarbonate, and then ice water. The solvent was removed from the dried (Na_2SO_4) extract and the residue was used in the next step.

Methyl Decyl-*9*-^{13}C Ether. The above mesylate in 10 mL of THF was added to a stirred slurry of $LiAlH_4$ (6.8 g) in 50 mL of dry THF and the reaction mixture was refluxed for 5 h. After hydrolysis with 130 mL of water and 90 mL of concentrated hydrochloric acid, the product was extracted into ether and the combined extracts were washed and then dried. Distillation gave the product in 77.3% yield (2.76 g, 16.0 mmol), bp 114–118 °C (14 mm).

Decyl-*9*-^{13}C Trimethylacetate.[72] To an acetonitrile (4.0 mL) solution of methyl decyl ether (2.76 g) and NaI (3.53 g) was added an acetonitrile (4.0 mL) solution of pivaloyl chloride (2.80 g) at 0 °C. After 24 h of stirring at room temperature, the reaction was quenched by the addition of aqueous $NaHSO_3$. After extraction with ether, followed by drying over Na_2SO_4, distillation gave the ester in 89.7% yield (3.48 g, 14.4 mmol), bp 144–150 °C (14 mm).

1-Decanol-*9*-^{13}C. To 0.58 g of lithium aluminum hydride in 27 mL of anhydrous THF was added a solution of the pivaloyl ester (3.48 g) in THF (22 mL). After stirring at room temperature for 12 h, the excess lithium aluminum hydride was decomposed with water (5.3 mL) and concentrated hydrochloric acid (5.3 mL). The mixture was extracted with ether and the combined extracts were washed with aqueous $NaHSO_3$, saturated sodium bicarbonate, and saturated brine and then dried (Na_2SO_4). The product was obtained in 89.6% yield (2.05 g, 12.9 mmol), bp 119–123 °C (14 mm). The structure and composition of this compound were confirmed as having only a trace amount of impurity shown by ^1H NMR.

(73) Rossi, R. *Synthesis* **1981**, 359.

Registry No. 1-Decanol-*1*-^{13}C, 87803-60-9; 1-decanol-*5*-^{13}C, 139408-57-4; 1-decanol-*9*-^{13}C, 139408-71-2; 1-decanol, 112-30-1; decanonitrile, 1975-78-6; 1-chlorononane, 2473-01-0; 4-hydroxybutyl methyl ether, 111-32-0; 1,4-butanediol, 110-63-4; 4-chlorobutyl methyl ether, 17913-18-7; 5-methoxypentanonitrile-*1*-^{13}C, 139408-58-5; *n*-pentyllithium, 3525-31-3; 1-bromopentane, 110-53-2; 1-methoxy-5-decanone-*5*-^{13}C, 139408-59-6; methyl 5-hydroxydecyl-*5*-^{13}C ether, 139408-60-9; 1-methoxy-*5*-^{13}C-decane-5-yl mesylate, 139408-61-0; methyl decyl-*5*-^{13}C ether, 139408-62-1; decyl-*5*-^{13}C trimethylacetate, 139408-63-2; 8-bromo-1-octanol, 50816-19-8; 1,8-octanediol, 629-41-4; 8-methoxy-1-octanol, 51308-90-8; 8-chlorooctyl methyl ether, 139408-64-3; 9-methoxynonanonitrile-*1*-^{13}C, 139408-65-4; 10-methoxy-2-decanone-*2*-^{13}C, 139408-66-5; 10-methoxy-2-decanol-*2*-^{13}C, 139408-67-6; 10-methoxy-2-decanomesylate-*2*-^{13}C, 139408-68-7; methyl decyl-*9*-^{13}C ether, 139408-69-8; decyl-*9*-^{13}C trimethylacetate, 139408-70-1; *n*-decanoic acid-*1*-^{13}C, 84600-66-8.